DEPARTMENT OF DEFENCE
DEFENCE SCIENCE & TECHNOLOGY ORGANISATION
DSTO

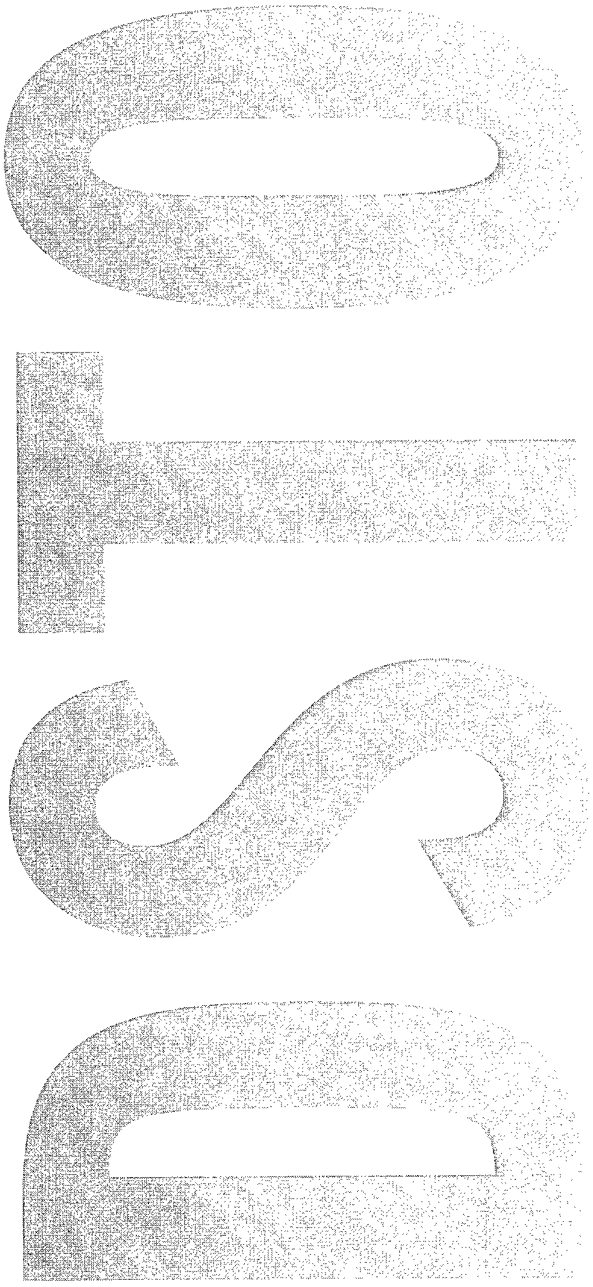

Theory Pertaining to Comparison and Calibration in an Experiment to Measure Acoustic Reflection Coefficients

David G. Blair

DSTO-TN-0417

Theory Pertaining to Comparison and Calibration in an Experiment to Measure Acoustic Reflection Coefficients

David G. Blair

Maritime Operations Division
Aeronautical and Maritime Research Laboratory

DSTO-TN-0417

ABSTRACT

For the purpose of analysing data to determine underwater acoustic reflection coefficients at low megahertz frequencies, relevant theory is developed. For a target that may be in the near field, the three-dimensional point spread function for image points close to the target, is derived for rather general arrays and waveforms. The model of the active system is extended to allow a coded signal, a spherical transmitter, and a transmitter not in the receiver array plane. Here and elsewhere, conditions of validity are carefully obtained. Conditions are derived under which a ball target (used for calibration in the experiment) behaves as a point reflector. The image of a rectangular target, described by an angle-dependent reflection coefficient, is obtained. The preceding results lead to an 'integral relationship,' or 'energy conservation' relationship, proved for a point target and conjectured to hold generally. It is shown how this result would enable one to analyse the experiment to determine absolute reflection coefficients.

RELEASE LIMITATION

Approved for public release

DEPARTMENT OF DEFENCE
DEFENCE SCIENCE & TECHNOLOGY ORGANISATION
DSTO

Published by

DSTO Aeronautical and Maritime Research Laboratory
506 Lorimer St
Fishermans Bend Vic 3207 Australia

Telephone: (03) 9626 7000
Fax: (03) 9626 7999

AR-012-280
March 2002

APPROVED FOR PUBLIC RELEASE

Theory Pertaining to Comparison and Calibration in an Experiment to Measure Acoustic Reflection Coefficients

Executive Summary

For minehunting in turbid waters, an underwater acoustic imaging device using low megahertz frequencies is being developed in industry following an initiative of DSTO. A problem is that, while rough surfaces are relatively easy to image, smooth surfaces (specular reflectors), when angled obliquely to the line of sight, tend to be invisible. To determine the extent of this problem, an experiment was performed, in which images were obtained for rectangular surfaces of different roughnesses inclined at various angles. Of particular interest is the diffuse component of the reflection from rather smooth surfaces; here 'diffuse' refers to the component that is spread over a wide range of angles of reflection. The diffuse component is of interest because, although weak, it may enable an image to be produced.

The present report describes a way in which the results can be analysed to produce the absolute reflection coefficient as a function of roughness and angle. From that functional relationship, together with the characteristics of the imaging system, one should be able to predict the circumstances in which certain mines cannot be imaged. More usefully, one should be able to predict how low the instrumentation noise must be made in order to image a given mine in given circumstances.

As stated, the present report describes a way of analysing the experimental results to produce the values of the reflection coefficient. For this purpose, various items of theory are developed. The key item in the theory is an 'integral relationship,' which expresses something akin to the conservation of energy in waves and fields. This relation says something like the following: that the 'energy' fed into the image by the receiving array is proportional to the 'energy' that is present in the image. The result is proved for a point target and is conjectured to hold generally.

(More precisely, the integral relationship asserts proportionality between two 'energies,' where, apart from slight modifications, these 'energies' are defined as follows. The first 'energy' is the squared voltage of the received signal, integrated over all the time during which the 'ping' is being received and summed over all sensor elements. Provided the beamforming is done by simple or weighted delay-and-add, it appears that this is the 'energy' that is 'fed' into the image in the beamforming process. The second 'energy' is the intensity of the image integrated over the three spatial dimensions.)

In the lead-up to the integral relation and the method of analysis, a number of results are obtained as follows. The three-dimensional image of a point target, allowed to be in the near field, is found under fairly general conditions. Extensions of the model of the imaging system are made, in order that the conditions of the experiment are

covered; the extensions include a spherical transmitter with its centre not in the receiver array plane. The conditions are derived under which a ball target—used for calibration in the experiment—behaves as a point reflector. Assuming the integral relationship, the image of a rectangular target, described by an angle-dependent reflection coefficient, is obtained.

Contents

1. Introduction

1.1 Background: The Reflectivity Experiment

The present work arose out of a problem in analysing the results of a certain experiment performed recently. That 'reflectivity experiment' aims to measure the acoustic reflection coefficient of various surfaces at low megahertz frequencies. Those surfaces, having the roughness characteristics of sandpaper, vary from acoustically smooth to quite rough (in the latter case, grain size ≈ half a wavelength). While the scattering from the former surface is approximately specular, the reflection from the latter surface is diffuse in the sense that considerable amounts of energy are reflected at angles of the order of 90° away from where a specular reflection would emerge. In this monostatic experiment, the surface is inclined with its normal at various angles to the incoming beam. The angles cover the entire range from 0° (normal incidence and reflection) to near 90° (grazing incidence).

The experiment has implications for the acoustic mine imaging (AMI) program that was initiated by the Maritime Operations Division (MOD) of DSTO and under which an AMI system is being developed by Thales Underwater Systems (TUS). Underwater acoustic imaging in general has been discussed by Murino and Trucco [2000]. Key aspects of the present AMI program have been discussed by various authors [Jones 1996; Blair and Jones 1998; Blair and Anstee 2000; and Maguer *et al.* 2000]. The implications of the reflectivity experiment for AMI concern the fact that smooth surfaces are hard to image when they are at any angle other than normal to the line of sight. But if the smooth (but not perfectly smooth) surface has a significant diffuse component in its reflection, imaging of that surface may still be possible. The strength of the diffuse reflection is therefore of great importance.

As a colleague has pointed out, when the diffuse scattering is small, success may depend on the level of volume reverberation being not too high. This is because the diffuse scattering events might not be seen above a certain set of double scattering events. The latter are those in which the sound is first scattered by a volume scatterer and second, reflected specularly from the solid surface.[1]

---

[1] A colleague has suggested that a near-specular reflector could be imaged by enlisting the aid of volume reverberation. In this proposal, the environment of the instrument would be seeded with suspended particles acting as scatterers. Then events in which the sound is doubly scattered—first by a particle and then by the reflecting surface—would return energy to the instrument even in the case of a perfect specular reflector (not oriented to return energy to the instrument by single scattering). However, imaging in this way does not seem promising—at least if delay-and-add beamforming is used—for the following reason. Given a path with double scattering, terminating in a given element, in a sense, beamforming fits to the data a path with single scattering. Accordingly, the peak in the image intensity—or the line or surface of peaks—is neither at the first nor at the second point of scattering, but at a greater range. Consideration of the many points of volume scattering and the many elements suggests that the 'image' of a particular reflection point on the solid surface will be quite blurred and of weak intensity.

However, in the context of a specular reflector, a high density of volume scatterers might be put to use in another way. Consider just paths of single scattering. Due to these paths, the 'water' would be 'seen' in the image and the interior of the solid would appear as a 'black' region; thus the surface

The reflectivity experiment will now be discussed in more detail. The experiment aims to determine the absolute reflection coefficient as a function of roughness and angle. From that functional relationship, together with the characteristics of the imaging system, one should be able to predict the circumstances in which certain mines cannot be imaged. More usefully, one should be able to predict how low the instrumentation noise must be made in order to image a given mine in given circumstances.

The reflectivity experiment was the result of collaboration between MOD, TUS and the Ocean Technology Group of the University of Sydney. The reflectivity experiment involves the acquisition of a large number of acoustic images, in each of which two targets are present. In most of these 'total images,' a comparison is made between two rectangular targets (often called *plates*). One of these, the 'standard' target, is kept at the same roughness (same target) and the same angle throughout the experiment. Thus for each pair, in principle one can find the ratio of the reflection coefficient of the variable or 'object' plate to that of the standard plate. In one (or in practice a few) of the total images, a comparison is made between the standard target and a small, smooth ball. The comparison with the ball is included for calibration purposes, to enable absolute reflection coefficients to be determined.

An initial analysis of the data from the experiment has been carried out [Madry 2000]. However contamination by noise has been a problem and it is believed that as a result, the initial method of analysis was well short of optimal in terms of the information extracted.

In AMI, the noise is due to (i) clutter, that is, distant sidelobes due to the random nature of the array, and (ii) instrumentation noise. Of the two noise sources, clutter is the more important. In the reflectivity experiment, because the targets are small (relatively small number of voxels), the amount of clutter is correspondingly reduced, and the noises from the two sources become more or less equal. Volume reverberation, due to scattering from suspended particles, is expected to be a significant source of noise when the particle density is very high. However this source is not significant in most of the AMI experiments to date, and in particular it is not significant in the reflectivity experiment.

It is believed that, subject to an assessment of the costs and risks, a more thorough analysis of the data is desirable. The purposes of this new analysis would be: (i) by subtraction and averaging, performed on the voxel intensities, to more fully remove the effects of noise, and (ii) to obtain further results, in particular the reflection coefficients. The latter result would follow from a theoretical analysis that would in particular, distinguish between the angular dependence of the reflection coefficient and that of the voxel intensities in the neighbourhood of the reflecting surface, by showing where 'further factors, such as $\cos i$,' enter (see below).

In regard to purpose (i), one would attempt to subtract off the instrumental noise (spatial average) and the clutter noise, leaving only the contribution arising from the reflection coefficient (with fluctuations). The instrumental noise is believed to be independent of position in the image, so its average value should be easy to estimate by examining regions in which both the clutter and the 'genuine' image intensity are negligible. The clutter varies with position relative to the target, as well as having spatial fluctuations that are effectively random. The hope would be to estimate its approximate value (apart from fluctuations) at

---

would be delineated. Before pronouncing on the viability of this concept, calculations would be required, particularly regarding the effect of second scatterings that arise due to the specular reflector.

each voxel near the target by making reasonable assumptions. The subtractions are not discussed further in this report.

In regard to the 'averaging' in purpose (i), when estimating the image amplitude A due to the reflection, and hence the reflection coefficient, clearly the more voxels that one averages over, the better, from the viewpoint of removing noise. In the initial analysis, Madry [2000] appears to have integrated the amplitude (or its square) over a surface parallel to the surface of the plate, that is, summed over a 2D array of voxels. It is hoped that a further reduction in noise can be achieved by performing a further integration along the direction perpendicular to the surface.[2] Integrals with respect to the coordinate n will appear naturally in Section 9; it is now seen that they are potentially useful.

In regard to purpose (ii), consider the voxel intensity, say at a point on the reflecting surface, as a function of the angle of incidence i. Naively one might think that this intensity is simply proportional to the reflection coefficient. However, in the absence of a theoretical account, it is not clear whether further factors, such as $\cos i$, enter into the proportionality. Such theory is therefore needed.

The present report has been written, mainly to serve purpose (ii) above, that is, to show how to analyse the experimental date to produce further results, in particular, values of the reflection coefficients. Theoretical argument backing the method of analysis is also provided. Some contribution towards purpose (i) is also made, by means of the extra integration discussed above.

1.2 The Present Report

We now describe the present report in more detail. The final outcome of the report is the proposing of a method for each of two stages of the experimental analysis (the plate-plate stage and the plate-ball stage). However, a prerequisite for that method is the development of an 'integral relationship' (described below); this development is also given in the report. For this in turn, it is found necessary to develop formulae for the image of each of the following: a point target, a small ball and planar surface that may be rough. Considerable care is taken to develop the conditions of validity applicable to each result.

The 'integral relationship' arises in the following way. When the two plates being compared are inclined *at different angles*, it is not obvious how the ratio, R_1 say, of the reflection coefficients is related to the set of voxel intensities in the neighbourhood of each of the two plates. Possibilities include the following. (i) The maximum voxel intensity along a line through each plate is determined, and the ratio of these two maxima is equated to R_1. (To reduce noise, one could integrate over an area parallel to the plate's surface, before determining the maximum, as discussed above.) (ii) A line integral of intensity, along a line perpendicular to each surface, is evaluated, and the ratio of these two integrals is equated to R_1. (To reduce noise, a volume integral could be taken.) (iii) Alternatively, it could be that, for a correct result, some other factor, such as $\cos i$ (as discussed above) needs to be included

[2] Note that the use of this integral requires some method of 'cutting off' the integral so that a false estimate of the instrumental noise or clutter does not lead to a divergent integral.

in the quantity determined in (i) or (ii) for each plate. To resolve this issue, it is conjectured, with a supporting argument, that a certain 'integral relationship,' similar to the energy conservation relationship in diffraction theory, holds.[3] (In fact factors such as described in possibility (iii) do enter, see Eqns 7.14 and 9.3.)

Essentially the integral relationship says that the 'energy' fed into the image by the receiving array is proportional to the 'energy' that is present in the image. (More precisely, the integral relationship asserts proportionality between two 'energies,' where, apart from slight modifications, these 'energies' are defined as follows. The first 'energy' is the squared voltage of the received signal, integrated over all the time during which the 'ping' is being received and summed over all sensor elements. Provided the beamforming is done by simple or weighted delay-and-add, it appears that this is the 'energy' that is 'fed' into the image in the beamforming process. The second 'energy' is the intensity of the image integrated over the three spatial dimensions.)

The layout of the report is as follows. Section 2 defines a model system similar to that used in the experiment, and sets out the image-forming (i.e. beamforming) theory for that model. The consideration of the differences of the experiment from the model, such as the location of the transmitter's centre away from the receiving array plane, is postponed to later in the report (Section 5). Building on Section 2, Sections 3 and 4 derive an expression for the image amplitude due to a point target (point spread function) that holds out through the first few angular and range sidelobes, for very general arrays and transmitted waveforms. Note that, while these expressions hold exactly under certain limiting conditions, in practice usually some of the conditions do not hold all that well and consequently the expressions suffer noticeable errors.

Section 5 considers differences[4] of the experimental arrangement from the model. These include the use of a spherical rather than a point transmitter, and the location of the transmitter's centre away from the receiving array plane. Coded signals such as chirps are also dealt with in this section. It is shown the three differences are readily incorporated into the theoretical formulae developed in Sections 3 and 4.

Section 6 treats the imaging of a small, smooth ball and shows that, under certain conditions—satisfied in the experiment—the ball is equivalent to a single point scatterer. Section 7 describes the response of a rough planar surface in terms of its angle-dependent reflection coefficient.

Section 8 puts forward as a conjecture the 'integral relationship' or 'energy conservation' relationship. Arguments are given that make this result plausible; in particular, the result is proved to hold for a point target. Assuming the integral relationship, the image of a rectangular target, described by an angle-dependent reflection coefficient, is obtained.

---

[3] This relationship was earlier proposed in an unpublished report: Blair, D.G. (2000), 'An Integral Relationship between Acoustic Properties of a Surface and Image Intensity' (DSTO Registry 600-1-62, item 24). In that report, only the briefest of outlines was given of the argument in support of the integral relationship.

[4] Another difference comes to mind, namely: it has not been established that the total target is equivalent to a collection of omnidirectional point scatterers with no double scattering events. But such equivalence is not actually used in the report for any of the targets: the point target, the ball and the rough planar surface.

Section 9 shows how certain results of this report, namely the results for a small, smooth ball and a rough planar surface (Sections 6 and 7), and the integral relationship (Section 8), can be applied to the analysis of the reflectivity experiment. Conclusions are given in Section 10, where further work on the integral relationship is foreshadowed.

2. Basic Model

For an imaging sonar system, Section 2 defines two models of different generality and sets out the image-forming theory for each model. We first consider the more general model of the two, the 'general basic model' (Section 2.1) and then specialise to the 'restricted basic model' (Section 2.2).

The consideration of the differences of the experimental arrangement from the latter model is postponed to Section 5. There it is shown that the theoretical results for a point target, derived in the first instance for the restricted basic model, are readily extended to apply to the experimental arrangement.

2.1 General Basic Model

Consider a sonar system that includes a spherical transmitter (in practice only a portion of a spherical surface), a receiving array and an omnidirectional point scatterer (see Fig. 1). The pressure produced at a receiver element due to the scattered wave is

$$p(t) = p_{\mathrm{tr\,ax}}\left(t - \frac{r_{\mathrm{out}} + r_{\mathrm{ret}}}{c}\right)\frac{bD_t}{(r_{\mathrm{out}} + b)r_{\mathrm{ret}}}a_0 \exp\left[-\frac{\alpha}{2}(r_{\mathrm{out}} + r_{\mathrm{ret}})\right]; \tag{2.1}$$

(see e.g. Blair and Anstee [2000], Sections 2, 3, with obvious corrections for a non-point transmitter and attenuation). Here the symbols have the following meanings:

$p(t)$ scattered wave pressure at the receiver element of interest (centre of front face)

$p_{\mathrm{tr\,ax}}(t)$ pressure at transmitter surface, on the axis of the transmitter, at time t

r_{out} distance of point target from front surface of spherical transmitter (outward path)

r_{ret} distance from point target to the receiver element of interest (return path)

b spherical radius of transmitter

D_t (amplitude) directivity of transmitter in target direction (equal to unity on the axis of the transmitter)

a_0 target strength of point target (usual target strength equals $20\log_{10}|a_0|$)

α (energy) attenuation coefficient (assumed independent of frequency)

It is understood that, in $p(t)$ and $p_{trax}(t)$, and in similar quantities below, the symbol refers to the *analytic signal*, except where the contrary is stated.

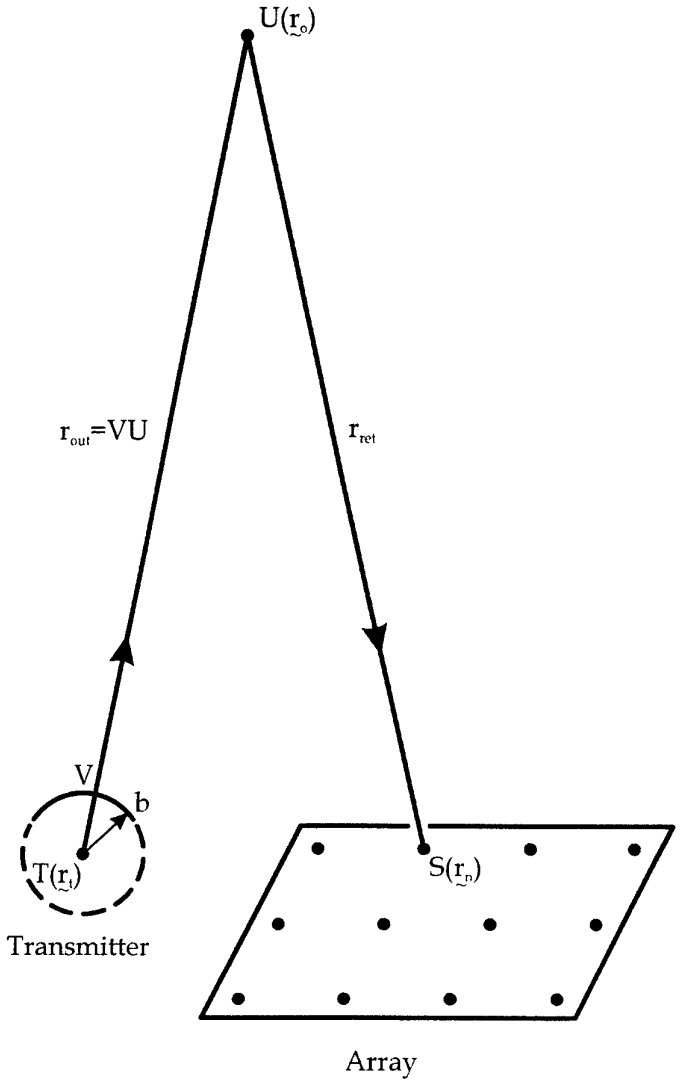

Figure 1: *The geometry of the sonar system. U is a point target. The vector location of each of the points T, U and S is given in parentheses.*

The pressure at the transmitter surface, on the axis of the transmitter,[5] will be written as

$$p_{\mathrm{trax}}(t) = p_0 \xi(t) \tag{2.2}$$

The central frequency of $\xi(t)$ is denoted by f_c and the bandwidth by B. In (2.2), p_0 is the maximum value of $|p_{\mathrm{trax}}(t)|$ over time, and $t = 0$ is chosen to be the time at which this maximum value occurs. (In the case of a pulse with a rectangular envelope, the maximum corresponds to a whole interval in t; then $t = 0$ is chosen at the centre of that interval.) Thus the maximum value of $|\xi(t)|$ is unity, and this occurs at $t = 0$:

$$|\xi(0)| = 1 \tag{2.3}$$

As implied above, $\xi(t)$ is the analytic signal.

For the time being we restrict attention to a non-correlated signal, that is, the use of a short pulse to obtain range resolution. The extension to a correlated pulse (chirp or coded signal) is readily made and is given in Section 5.3.

The array considered is two-dimensional (2-D) and the element faces lie in a common plane; the xy plane is taken to be parallel to this plane. The maximum directivity of each element is taken to be in the z or broadside direction. Then the voltage at any receiver element is

$$E(t) = \sigma D_r p(t) \tag{2.4}$$

Here σ is the sensitivity of the element (in volts per pascal) and D_r is the directivity of the element in the direction of the target; D_r is unity in the broadside direction.

For the nth element we combine (2.1) and (2.4) to yield

$$E_n(t) = \sigma_n D_{rn} p_{\mathrm{trax}}\left(t - \frac{r_{\mathrm{out}} + r_{\mathrm{ret}\,n}}{c}\right) \frac{bD_t}{(r_{\mathrm{out}} + b) r_{\mathrm{ret}\,n}} a_0 \exp\left[-\frac{\alpha}{2}(r_{\mathrm{out}} + r_{\mathrm{ret}\,n})\right] \tag{2.5}$$

We shall rewrite this expression in terms of $\mathbf{r}_t$, the location of the spherical centre of the transmitter, $\mathbf{r}_0$, the location of the point scatterer and $\mathbf{r}_n$, the location of the centre of the front face of the nth element. Thus

[5] It is assumed that the beam pattern of the transmitter across its surface is the same as the beam pattern at the distances where the targets are located.

$$E_n(t)=\sigma_n D_{rn}\, p_{\mathrm{tr}\,ax}\left(t-\frac{|\mathbf{r}_0-\mathbf{r}_t|-b+|\mathbf{r}_0-\mathbf{r}_n|}{c}\right)\frac{bD_t}{|\mathbf{r}_0-\mathbf{r}_t||\mathbf{r}_0-\mathbf{r}_n|}a_0\times \exp\left[-\frac{\alpha}{2}\left(|\mathbf{r}_0-\mathbf{r}_t|-b+|\mathbf{r}_0-\mathbf{r}_n|\right)\right] \tag{2.6}$$

The complex *image amplitude* at $\mathbf{r}$ is obtained by adding the voltages evaluated at suitable times:

$$A(\mathbf{r})=\sum_n w_n E_n\left[\left(|\mathbf{r}-\mathbf{r}_t|-b+|\mathbf{r}-\mathbf{r}_n|\right)/c\right]; \tag{2.7}$$

this is called the *image-forming* (or beamforming) *equation*. The usual image amplitude is then $|A(\mathbf{r})|$. In (2.7), w_n (taken to be real) is a weighting factor. We shall consider only the case where w_n varies in a non-rapid way with the position of the element in the array. The following normalisation is imposed:

$$\sum_n w_n = N \tag{2.8}$$

where N is the total number of elements. (In the reflectivity experiment the shading is uniform: $w_n = 1$.)

In the case where there are a number of point targets, the pressure $p(t)$ becomes the sum of a number of terms, each given by the right-hand side of (2.1); and the voltage becomes the sum of terms, each given by (2.5) or (2.6). Equation (2.7) still gives the image amplitude; note that the image amplitude $A(\mathbf{r})$ is the sum of the image amplitudes due to the various point targets. The corresponding summation result does not in general hold for the *image intensity* defined by $I(\mathbf{r})=|A(\mathbf{r})|^2$.

2.2 Restricted Basic Model

Next we obtain the 'restricted basic model' by specialising the above more general model in two ways. First, we consider the case where the transmitter is a point. Second, we consider the point transmitter to be on the front plane of the receiving array; we shall choose the origin at the transmitter; thus $\mathbf{r}_t = 0$ (see Fig. 2). It will be convenient also to require that the transmitter be not too far from the centre of the array. The criterion chosen is that

$$|\mathbf{r}_c-\mathbf{r}_t| \le \tfrac{3}{2}\left(\tfrac{1}{2}L\right) \tag{2.9}$$

where $\mathbf{r}_c$ is the centre of the array and L is the maximum dimension across the array. Thus the transmitter lies either within the array or not far outside it. (In Eqn 2.9, $\mathbf{r}_t$ is retained, rather than being replaced by zero, for ease of comparison with later results.)

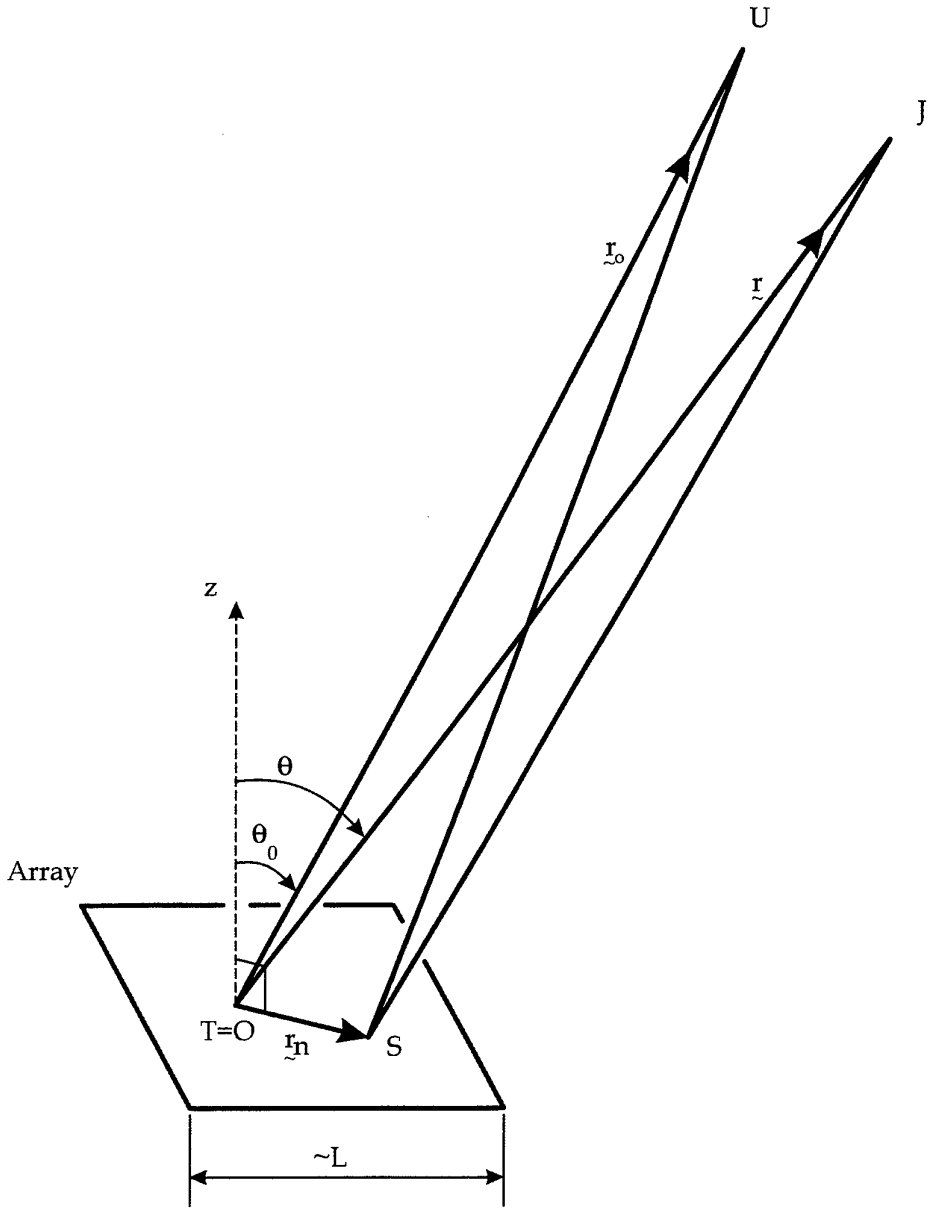

Figure 2: *Specifying the location of the point target U and a particular image point J, for the model of Section 2.2. In the model, the point transmitter T is in the plane of the array and the origin is chosen there. The nth element is at S.*

For a point transmitter, Equation (2.6) then becomes

$$E_n(t)=\sigma_n D_{rn} b\, p_{\mathrm{trax}}\left(t-\frac{r_0+|\mathbf{r}_0-\mathbf{r}_n|}{c}\right)\frac{D_t}{r_0|\mathbf{r}_0-\mathbf{r}_n|}a_0\exp\left[-\frac{\alpha}{2}\left(r_0+|\mathbf{r}_0-\mathbf{r}_n|\right)\right] \tag{2.10}$$

Here it is understood that the product $bp_{\mathrm{trax}}(\cdot)$ (and similarly bp_0 in Eqn 2.12) is to be treated as a unit, which approaches a finite value in the limit in which $b\to 0$ while the acoustic power emitted by the transmitter is held constant. Making the approximation that the directivity $D_{rn} = D_r$ is the same for all elements, and using (2.2), we rewrite (2.10) as

$$E_n(t)=\sigma_n D_r a_0 H\,\xi\left(t-\frac{r_0+|\mathbf{r}_0-\mathbf{r}_n|}{c}\right) \tag{2.11}$$

where

$$H=\frac{bp_0 D_t}{r_0|\mathbf{r}_0-\mathbf{r}_n|}\exp\left[-\frac{\alpha}{2}\left(r_0+|\mathbf{r}_0-\mathbf{r}_n|\right)\right] \tag{2.12}$$

Actually H depends on n, but we now ensure that H is independent of n by making the simplifying approximation:

$$H=\frac{bp_0 D_t}{r_0^2}\exp(-\alpha r_0) \tag{2.13}$$

A sufficient condition for this approximation to be accurate is obtained by considering the approximately plane wavefronts of spherical waves emanating from $\mathbf{r}_0$; the path to $\mathbf{r}_n$ is replaced by the path to $\mathbf{r}_t$. The sufficient condition is that both[6,7]

$$r_0 >> L \quad \text{and} \quad \alpha\left[\tfrac{1}{4}L\sin\theta_0+\tfrac{1}{2}|\mathbf{r}_c-\mathbf{r}_t|\sin\theta_0\right]<<1 \tag{2.14}$$

Here $\mathbf{r}_0=(r_0,\theta_0,\phi_0)$ in spherical polars (see Fig. 2; also Fig. 3 below). (We have used the assumption that $\mathbf{r}_c-\mathbf{r}_t$ lies in the plane of the receiving array. The inequality $r_0 >> L$ in

---

[6] As used in this report, the symbols $\lesssim$, $<<$, etc. normally represent order relations, similar to $O(f)$ and $o(f)$, where f is some function of the independent variables. The details are indicated in these brief notes. The relations are always between positive quantities. $f\gtrsim g$ means 'f/g is bounded below by a positive number.' $f<<g$ means $f/g\to 0$. $f\simeq g$, in practice written as $f=g$ or 'f is given by g,' means $f/g\to 1$. Additionally it is implied that the relationship concerned ($\lesssim$, $<<$, etc.) holds *uniformly* with respect to all parameters (as in the uniform convergence of series).

[7] Sometimes, as in (2.14), a numerical factor is inserted in relations such as $f<<g$. In the present case the basic assertion is of the form '$h\simeq j$ if $f<<g$'. The numerical factor is inserted in $f<<g$ in order to give a stronger indication regarding when the approximation $h=j$ is accurate.

Eqn 2.14 obviously suffices to justify the approximation made to the spherical spreading factor in 2.13.) Because of (2.9), the second inequality in (2.14) may be replaced as a sufficient condition by $\frac{5}{8}\alpha L \sin\theta_0 << 1$. Thus (2.14) can be replaced[8] as a sufficient condition by

$$r_0 >> L \quad \text{and} \quad \tfrac{5}{8}\alpha L \sin\theta_0 << 1 \tag{2.15}$$

The image amplitude (2.7) becomes

$$\begin{aligned} A(\mathbf{r}) &= \sum_n w_n E_n\left[\left(r + |\mathbf{r} - \mathbf{r}_n|\right)/c\right] \\ &= D_r a_0 H \sum_n w_n \sigma_n \, \xi\left(\frac{r - r_0 + |\mathbf{r} - \mathbf{r}_n| - |\mathbf{r}_0 - \mathbf{r}_n|}{c}\right) \end{aligned} \tag{2.16}$$

We next deal with σ_n. As part of the model, we assume that the sensitivities σ_n, in each local area of the array, have the same distribution as in the whole array. Then (as long as the number of elements N is very much greater than one—a condition not hard to meet), sums of the form $\sum_n \sigma_n f_n$ and $\sum_n \sigma_n^2 f_n$ may be evaluated as

$$\sum_n \sigma_n f_n = \overline{\sigma} \sum_n f_n \quad \text{and} \quad \sum_n \sigma_n^2 f_n = \sigma_{\text{rms}}^2 \sum_n f_n \tag{2.17}$$

provided that f_n does not vary rapidly with the position of n. (Here $\overline{\sigma}$ and σ_{rms} are the mean and root-mean-square values of σ_n). The reason is as follows. Consider the part of the summation that covers a small (but not too small) interval or region of the position of n. In this partial sum, f_n is a constant to a good approximation, and so it may be taken outside the summation sign. But with interval size chosen not too small, there are *many* elements contributing to the partial sum, so that σ_n (or σ_n^2) may be replaced by its average. Putting together the partial sums and recalling our assumption that $\overline{\sigma}$ and σ_{rms} are constant over the array, we obtain the result (2.17). Equation (2.16) then becomes

$$A(\mathbf{r}) = D_r a_0 H \, \overline{\sigma} \sum_n w_n \xi\left(\frac{r - r_0 + |\mathbf{r} - \mathbf{r}_n| - |\mathbf{r}_0 - \mathbf{r}_n|}{c}\right) \tag{2.18}$$

---

[8] It also follows that H is independent of the transmitter location (subject to 2.9). (To reach this conclusion we make the reasonable assumption that D_t changes negligibly when the direction of the target from the transmitter changes by a small amount of order L/r_0 .)

3. Angular Dependence of the Point Spread Function

In Sections 3 and 4, for the restricted basic model, a formula is derived for the point spread function (PSF) that holds out through the first few angular and range sidelobes, for very general arrays and transmitted waveforms. Section 3 derives the *angular* dependence of the PSF; Section 4 will extend this result to obtain the 3-D dependence. (For ease of presentation, Section 3 also assumes that the transmitted waveform is a short *toneburst*.)

Section 3 begins by considering two 'close-to-target' approximations. It is thus shown that, under certain conditions, the far-field expansion for the point spread function is accurate to first order even though the target is, in general, not in the far field. As expected from this similarity to the far field, the formula for the PSF referred to above involves a Fourier relationship to the distribution of element strength.

Recall that a later goal is to derive an integral relationship relevant to the reflectivity experiment. In the latter, the array is sparse and random. Now, of the two integrals in the integral relationship, one is the image intensity integrated over volume. For a sparse, random array, with a point target, the intensity of the distant sidelobes is (in some cases) constant with angular displacement, on average. Because of this, the spatial integral shows a kind of divergence: the integral is much larger than would be obtained from the inner lobes alone. Such a large integral is not what we seek for the integral relationship. We deal with this problem by introducing a modified PSF that has a Fourier relationship with a *smoothed* version of the element strength distribution. The modified PSF does not have the troublesome distant sidelobes.

3.1 Close-to-Target Approximation

It has been noted before [Smith *et al.* 1991 ; Blair and Anstee 2000, p. 36], from simulations, that the angular beam pattern of a point target in the near field is, at least approximately, the same as in the far field. Others [Steinberg 1976, p. 322; Murino and Trucco 2000] have shown asymptotic equality between the two patterns, but have shown this only within the context of using the Fresnel approximation. We shall show that, under certain limiting conditions, not requiring the Fresnel approximation, the two patterns are the same.

First consider the *far-field expansion* of Equation (2.16). Expressing $|\mathbf{r}-\mathbf{r}_n|$ and $|\mathbf{r}_0-\mathbf{r}_n|$ as square roots and expanding in descending powers of r and r_0, we obtain for the point spread function (PSF), to second order,

$$A_0(\mathbf{r}) = D_r a_0 H \sum_n w_n \sigma_n \xi\left(\frac{1}{c}\left\{2(r-r_0)-(\hat{r}-\hat{r}_0)\cdot\mathbf{r}_n+\frac{1}{2r}\left[r_n^2-(\hat{r}\cdot\mathbf{r}_n)^2\right]-\frac{1}{2r_0}\left[r_n^2-(\hat{r}_0\cdot\mathbf{r}_n)^2\right]\right\}\right) \tag{3.1}$$

Of the four terms in the curly brackets, consider the second term, which is the first-order term. Truncation after this term gives exactly the far-field angular beam pattern which, in the case of a narrow-band signal ($B << f_c$), is essentially the Fourier transform of the array

distribution. (On the left-hand side the subscript 0 has been added to $A(\mathbf{r})$ to emphasise that this is the PSF, i.e. the image amplitude due to a *point* target.)

Now, instead of the far-field expansion, consider an expansion of (2.16) in terms of the displacement $\mathbf{r}-\mathbf{r}_0$ of the image point from the target point. First we obtain the expansion when carried out as a Taylor series in terms of the *Cartesian* components of $\mathbf{r}-\mathbf{r}_0$ (*Cartesian close-to-target expansion*). The result to second order is

$$A_0(\mathbf{r}) = D_r a_0 H \sum_n w_n \sigma_n \xi\left(\frac{1}{c}\left\{(r-r_0)+\frac{(\mathbf{r}_0-\mathbf{r}_n)\cdot(\mathbf{r}-\mathbf{r}_0)}{|\mathbf{r}_0-\mathbf{r}_n|}+E_1\right\}\right) \tag{3.2}$$

with

$$E_1 = \tfrac{1}{2}\frac{|\mathbf{r}_0-\mathbf{r}_n|^2|\mathbf{r}-\mathbf{r}_0|^2-[(\mathbf{r}_0-\mathbf{r}_n)\cdot(\mathbf{r}-\mathbf{r}_0)]^2}{|\mathbf{r}_0-\mathbf{r}_n|^3}$$

This time there is no zero-order term (i.e. zero-order in $\mathbf{r}-\mathbf{r}_0$); the first and second terms in the curly brackets together give the first-order contribution.

Second, consider $\mathbf{r}$ to be expressed as spherical polar coordinates (r,θ,ϕ), where the polar direction z is broadside to the array and θ is the co-latitude (see Fig. 3). This time, after going back again to Equation (2.16), we expand in terms of $r-r_0$, $\theta-\theta_0$ and $\phi-\phi_0$ (*spherical polar close-to-target expansion*). The result from this, to *first* order, is

$$A_0(\mathbf{r}) = D_r a_0 H \sum_n w_n \sigma_n \xi\left(\frac{1}{c}\left\{(r-r_0)+\frac{[r_0-r_n\sin\theta_0\cos(\phi_0-\phi_n)](r-r_0)+E_2}{|\mathbf{r}_0-\mathbf{r}_n|}\right\}\right) \tag{3.3}$$

with

$$E_2 = r_0 r_n[-\cos\theta_0\cos(\phi_0-\phi_n)(\theta-\theta_0)+\sin\theta_0\sin(\phi_0-\phi_n)(\phi-\phi_0)]$$

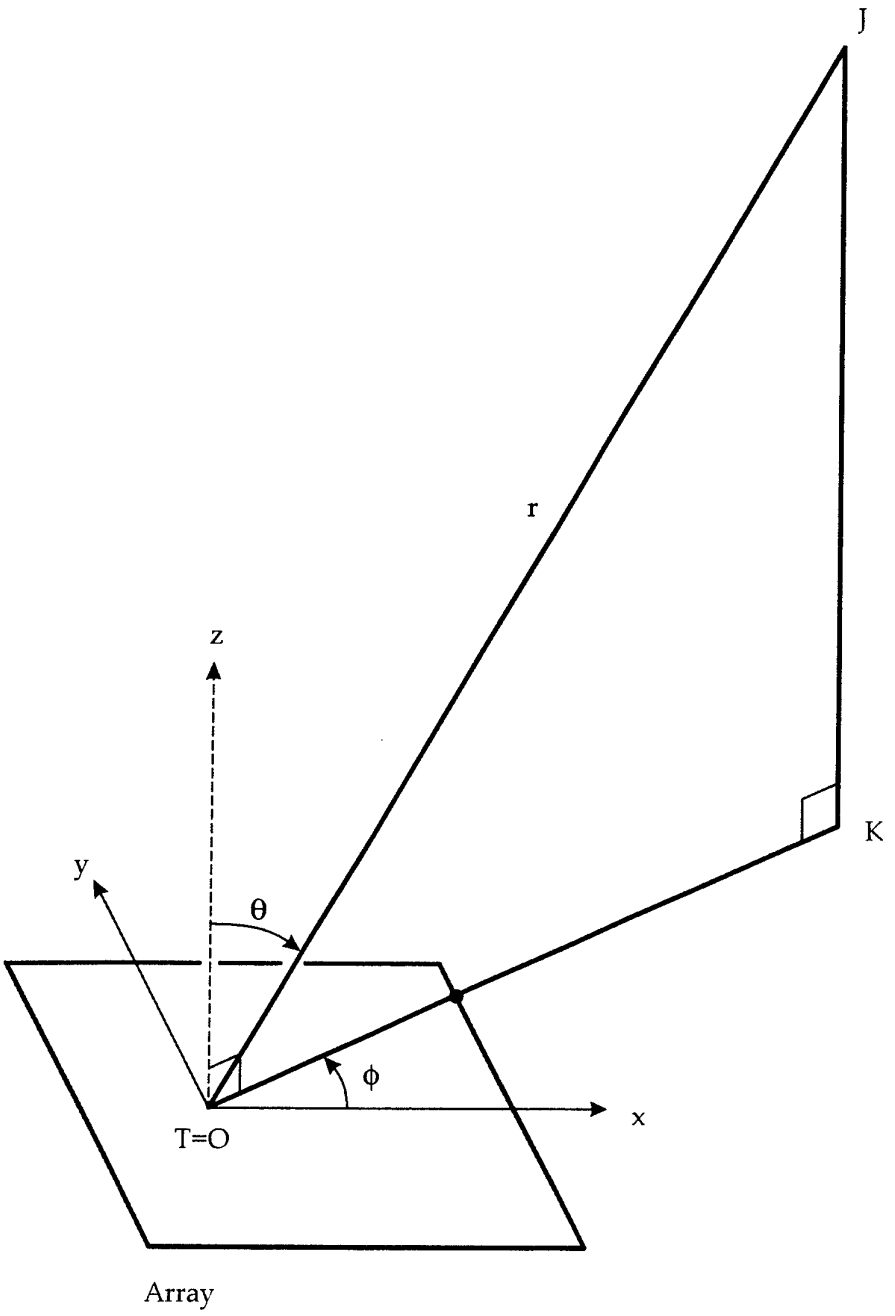

Figure 3: *Specifying the spherical polar coordinates* (r, θ, ϕ) *of the image point J, again for the model of Section 2.2. OK is the projection of OJ onto the plane of the array.*

Consider the three expansions, (3.1), (3.2) and (3.3), but each truncated at first order. While the three truncated expansions are not quite equal, the differences can be shown to be *of a higher order than the retained terms.* (The proof is omitted.) To state the result more

precisely, for the rest of this paragraph, let us adopt the convention that each of '(3.1)', '(3.2)' and '(3.3)' refers to just the contents of the curly brackets in the respective equation. A 'truncated' version of any of these refers to truncation at first order. The result is fourfold. First, for displacements $\mathbf{r}-\mathbf{r}_0$ in the radial direction (parallel to $\mathbf{r}_0$), the difference between truncated (3.2) and truncated (3.1) is small compared to the term $2(r-r_0)$ in (3.1). Second, for displacements $\mathbf{r}-\mathbf{r}_0$ along the sphere $r=r_0$, the difference between truncated (3.2) and truncated (3.1) is small compared to the angular term $-(\hat{r}-\hat{r}_0)\cdot\mathbf{r}_n$ in (3.1). Third and fourth, the analogous results hold for the comparison of the expression (3.3) with (3.1).

These findings give us confidence to proceed to the next step, that of showing that, under appropriate conditions, not necessarily far-field, the expansion (3.1), truncated at first order, is accurate. To find these conditions, we need to determine when the quantity in curly brackets is given correctly, not just in relative terms but to *within a small fraction of a wavelength*. We need conditions under which the errors in both (i) the second- and higher-order terms, and (ii) the differences in the first-order terms, are negligible on the wavelength scale. This question has been investigated; the result is as follows (proof omitted).

Even when $\mathbf{r}$ and $\mathbf{r}_0$ are not in the far field, the *far-field expansion (3.1), truncated at first order, is accurate for the purpose of calculating the image amplitude,* provided that four conditions hold. Those conditions are:

(i) $\mathbf{r}$ is no further away in angle from $\mathbf{r}_0$ than the first few sidelobes;

(ii) θ_0 is not near 90°;

(iii) $\lambda \ll L \ll r_0$; and (3.4)

(iv) a restriction on the ranges holds as follows:

(a) $|r-r_0| \ll \lambda(r_0/L)^2$ in the case $r_0 \lesssim L^2/\lambda$;

(b) $r \gg L^2/\lambda$ in the case $r_0 \gg L^2/\lambda$.

Note that the restriction on range, $r_0 \gg L$, in (iii) is much weaker[9] than the far-field restriction $r_0 \gg L^2/\lambda$. The two cases in (iv) are respectively the cases of the target in the near and the far field. From Steinberg [1976], the size of the focal zone based on r_0 is $7\lambda(r_0/L)^2$. Thus the condition (iv)(a) on $r-r_0$ is precisely the requirement that r must lie well within that focal zone.

[9] The restriction $r_0 \gg L$ is also considerably weaker than the condition associated with the validity of the Fresnel approximation: see above Equation (3.16).

3.2 Derivation of Point Spread Function (Angular)

3.2.1 General

We have seen that, under the conditions (3.4) (essentially, image point close to the point target), Equation (3.1) holds to first order. Then (2.18) becomes

$$A_0(\mathbf{r}) = D_r a_0 H \bar{\sigma} \sum_n w_n \xi\left\{\frac{1}{c}[2(r-r_0)-(\hat{r}-\hat{r}_0)\cdot\mathbf{r}_n]\right\} \tag{3.5}$$

where the $\bar{\sigma}$ is explained at Equation (2.17). In the present Section 3 we restrict attention to the case in which (i) the image point lies on the sphere $r = r_0$, and (ii) the signal is a toneburst, given by

$$\xi(t) = \exp(j2\pi ft)\,\mathrm{rect}(t/T) \tag{3.6}$$

where T is the duration of the burst; the burst has frequency f and wavelength λ. (Both the restrictions (i) and (ii) will be removed in Section 4.) Thus (3.5) becomes

$$A_0(\mathbf{r}) = D_r a_0 H \bar{\sigma} \sum_n w_n \exp\left[-j2\pi\frac{1}{\lambda}(\hat{r}-\hat{r}_0)\cdot\mathbf{r}_n\right]\mathrm{rect}\left[\frac{1}{cT}(\hat{r}-\hat{r}_0)\cdot\mathbf{r}_n\right] \tag{3.7}$$

We now drop the rect factor; the condition for this will be obtained in the paragraph containing (3.16). Then we may write

$$A_0(\mathbf{r}) = D_r a_0 H \bar{\sigma} \int \exp\left[-j2\pi\frac{1}{\lambda}(\hat{r}-\hat{r}_0)\cdot\mathbf{R}\right] w(\mathbf{R}) g(\mathbf{R}) d^2R \tag{3.8}$$

where the shading factor $w(\mathbf{R}) = w_n$ varies with position in a non-rapid way (as discussed near Eqn 2.7), the quantity

$$g(\mathbf{R}) = \sum_n \delta(\mathbf{R}-\mathbf{r}_n) \tag{3.9}$$

is the (unsmoothed, unweighted) *element number density,* and $\mathbf{R}$ is a 2-D vector in the xy plane.

Equation (3.8) may be rewritten in terms of the *weighted* element number density, defined as

$$g^w(\mathbf{R}) = w(\mathbf{R}) g(\mathbf{R}) \tag{3.10}$$

We define the Fourier transform $G^w(\boldsymbol{\kappa})$ of the latter, via the definition of the Fourier transform of a general function $h(\mathbf{R})$, namely

$$\mathsf{F}[h(\mathbf{R})] = H(\boldsymbol{\kappa}) = \int e^{-j2\pi\boldsymbol{\kappa}\cdot\mathbf{R}} h(\mathbf{R}) d^2R \tag{3.11}$$

Then (3.8) becomes

$$A_0(\mathbf{r}) = D_r a_0 H \overline{\sigma}\, G^w(\boldsymbol{\kappa}_2) \tag{3.12}$$

where

$$\boldsymbol{\kappa}_2 = \mathsf{P}_{xy} \frac{1}{\lambda}(\hat{r} - \hat{r}_0) \tag{3.13}$$

and the operator P_{xy} means projection onto the xy plane. $\boldsymbol{\kappa}_2$ is expressed in a natural way by using u and v as the angular coordinates, where

$$\begin{aligned} u &= \frac{x}{r} = \sin\theta\cos\phi \\ v &= \frac{y}{r} = \sin\theta\sin\phi \end{aligned} \tag{3.14}$$

Thus

$$\begin{aligned} \boldsymbol{\kappa}_2 &= \frac{1}{\lambda}\left[\frac{1}{r}(x,y) - \frac{1}{r_0}(x_0,y_0)\right] \\ &= (1/\lambda)(u-u_0, v-v_0) \end{aligned} \tag{3.15}$$

where u_0 and v_0 refer to the target direction.

The key result, (3.12) or (3.8), establishes the point spread function $A_0(\mathbf{r})$ and the weighted element density $w(\mathbf{R})g(\mathbf{R})$ as *Fourier transforms of each other* (with multiplicative constants inserted). This result will reappear at Equation (3.23) for a smoothed array, expressed in terms of the directivity. The smoothed result will again appear at Equation (4.19) but generalised to cover the three-dimensional PSF. The basic result (3.12), expressing the Fourier relationship, is of course not new in the case of the far field. It is given, for example, by Ziomek [1985, p. 38] (who actually considers the more general case of 3-D arrays). That result is given also by Steinberg [1976, pp.12, 15] in the cases of the 1-D and the 2-D array; only for the former does he make the Fourier connection explicit. What is new in (3.12) and (3.23) is that the Fourier relation holds also in the *near field* subject to certain conditions, chief of which is that the image point **r** lies in the first few angular lobes. Note also that the 'near field' in which the result holds covers not merely the ranges for which the Fresnel approximation (the retaining of one term beyond the far-field term [see Ziomek 1985, p. 37; Steinberg 1976, p. 36]) is valid, but covers all the region $r_0 >> L$ (see (iii) of Eqn 3.4).

It remains to determine the condition under which the rect factor can be dropped. Within the first few sidelobes, the argument of the exp in (3.7) is no greater than order unity; thus we have

$$\left|\lambda^{-1}(\hat{r}-\hat{r}_0)\cdot\mathbf{r}_n\right| \lesssim 1 \tag{3.16}$$

The condition required is that the argument of rect in (3.7) have absolute value less than ½. We impose the requirement that the argument be *small* compared to unity; this is a *sufficient* condition.[10] Combining this with (3.16), we obtain the sufficient condition $(1/cT)\lambda << 1$, which may be written as

$$fT >> 1 \tag{3.17}$$

3.2.2 Sparse Arrays

In a sparse array the spacing between elements is large compared to half a wavelength – the latter being the spacing that, in a periodic array, is just sufficient to always avoid grating lobes. A sparse array may be periodic or random, or it may be neither of these. Provided the array is not extremely sparse, the first few lobes[11] of the intensity point spread function (PSF) are essentially the same as for a filled array (or an aperture) (see Fig. 4). Consider first the periodic case, beginning with the monofrequency subcase: then, as the angular displacement increases, eventually the sidelobes increase again in height and grating lobes are produced. In the wideband subcase, each grating lobe is 'smeared'; its height is reduced but it extends over a greater interval of angles. Second, consider random arrays: these have been discussed by Steinberg [1976] and Steinberg and Subbaram [1991]. For these arrays, after the first few sidelobes the sidelobe level, on average, either: (i) stays constant, as in the monofrequency, far-field case; or (ii) in the wideband case (as discussed by Blair *et al.* [1994]) the level continues to decrease but considerably more slowly than for the filled array. In each of cases (i) and (ii), superimposed on the trend described are random fluctuations, comparable in size to the sidelobe intensity itself (Fig. 4). In the monofrequency case the average sidelobe intensity is $1/N$ times the peak intensity.

[10] The reason for imposing this stronger requirement is that the resulting condition then continues to be the condition of validity in the case of a more general signal $\xi(t)$ (Section 4).

[11] Here the term 'lobe' includes both the main lobe and sidelobes.

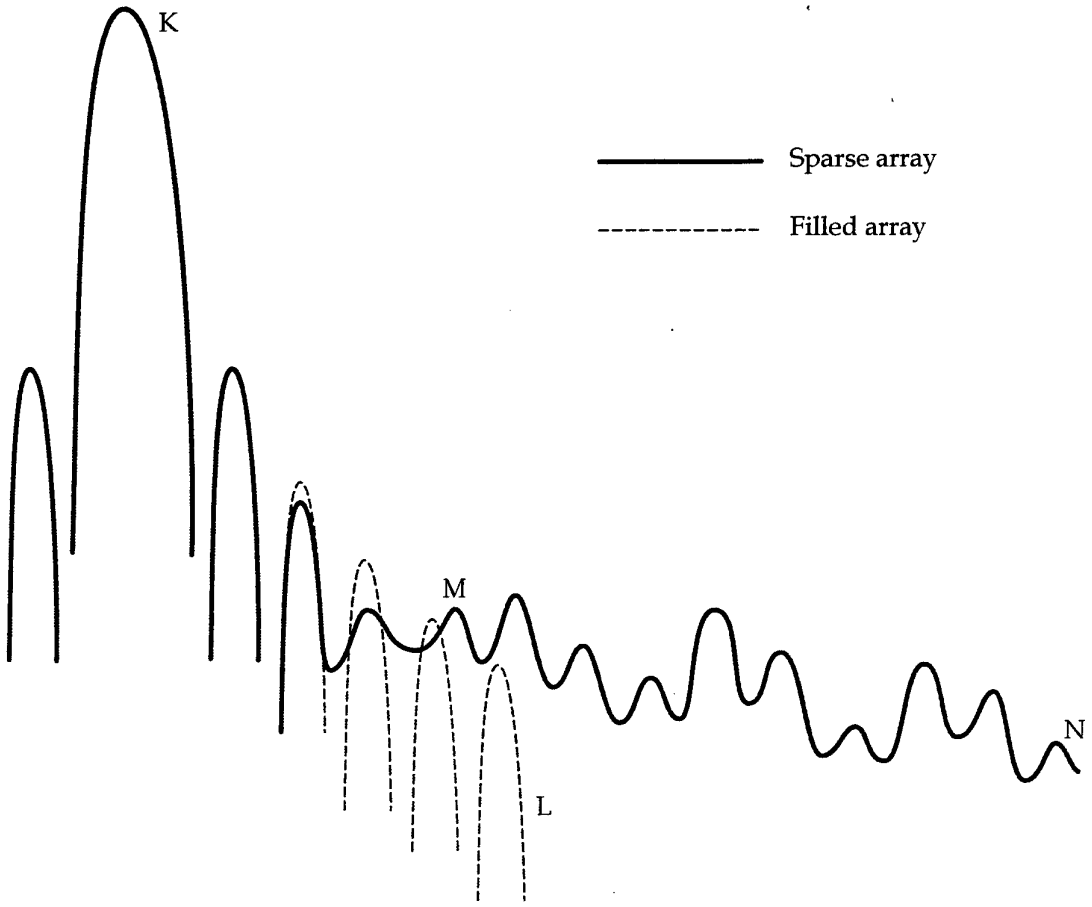

Figure 4: *Intensity beam pattern of a sparse array, compared to a filled array of the same aperture. A slice through the angular beam pattern is shown. Point target is at K. A decibel scale is used. See text.*

For the purposes of the integral relationship, *it will be sufficient to represent the PSF accurately in the first few angular lobes.* Because of this, for the present we restrict attention to $\mathbf{r}$ lying no further from $\mathbf{r}_0$ than the first few angular sidelobes. Then even for a sparse array, the angular beam pattern is the same as for the aperture.[12] This result is subject to the condition that, in the sparse array, N is quite large compared to one—this condition is not very demanding. Then $g(\mathbf{R})$ *may be replaced by a smoothed version of itself, to be denoted by* $\overline{g}(\mathbf{R})$. $\overline{g}(\mathbf{R})$ is the *smoothed* (or local) *element density.* We define also the weighted, smoothed element density $\overline{g}^{w}(\mathbf{R}) = w(\mathbf{R})\overline{g}(\mathbf{R})$. $\overline{G}(\boldsymbol{\kappa})$ and $\overline{G}^{w}(\boldsymbol{\kappa})$ are defined as the transforms of $\overline{g}(\mathbf{R})$ and $\overline{g}^{w}(\mathbf{R})$ respectively.

[12] This result is obtainable—at least for the far-field, monofrequency case—from Steinberg [1976, pp. 142-144].

Thus, at least in the near lobes, Equation (3.12) becomes

$$\overline{A}_0(\mathbf{r}) = D_r a_0 H \overline{\sigma}\, \overline{G}^{w}(\boldsymbol{\kappa}_2) \tag{3.18}$$

The bar on the symbol A_0 is explained below (3.19). Equation (3.18) is the fundamental result of Section 3. It will later be written in a different guise as Equation (3.29); the conditions for the validity of these two formulae are noted at that point.

Consider for the moment the case where the elements are distributed *uniformly* over the aperture. (This case includes, among other cases: (i) a sparse, random array with uniform probability distribution, and (ii) an array of elements lying on a square lattice, provided in both cases that there is no shading of any kind.) (Non-uniform cases will be discussed in Section 3.2.3.) Then we may take

$$\begin{aligned} \overline{g}(\mathbf{R}) &= N/S_{\text{ap}} \qquad \mathbf{R} \text{ in the aperture} \\ &= 0 \qquad\qquad \text{otherwise} \end{aligned} \tag{3.19}$$

where S_{ap} is the area of the aperture.

The replacement of $g(\mathbf{R})$ by $\overline{g}(\mathbf{R})$ is important. Without it, the volume integral of the image intensity would, for a sparse array, be dominated by the distant sidelobes—whether they be grating lobes, as in the case of a regular array, or the 'smeared-out grating lobes,' as in the case of a random array. The expression for $\overline{A}_0(\mathbf{r})$ in (3.18) (dependent on $\overline{g}$ or $\overline{G}$), when evaluated in the distant sidelobes, is small and the volume integral in this region no longer dominates the integral over all space. The notation $\overline{A}_0(\mathbf{r})$, including a bar, is so far defined only for the first few lobes. We now extend the notation to *other* values of **r**, to mean a quantity that is zero or negligible.[13] Then clearly Equation (3.18) holds, not just in the near lobes, but at all **r** (in the sense that the error is small compared to the peak value of $\overline{A}_0(\mathbf{r})$).

Let us write down the criterion for an array to be *well-filled*, i.e. sufficiently dense so that the system does not 'come close' to exhibiting grating lobes (either simple grating lobes or the smeared-out grating lobes characteristic of sparse, random arrays). The criterion for this is that the mean separation of neighbouring elements is small compared to the wavelength λ_c (compare the customary critical value $\frac{1}{2}\lambda$). (We write λ_c in place of λ, anticipating the more general ξ to be introduced at Eqn 4.4.) Thus, since the array is 2-D, the grating lobe criterion is that

$$L^2/N << \lambda_c^2, \quad \text{i.e.} \quad N\lambda_c^2/S_{\text{ap}} >> 1 \tag{3.20}$$

---

[13] For reasons that will become apparent in Section 8, we also require that the angular *integral* of $\left|\overline{A}_0(\mathbf{r})\right|^2 \cos\theta$ in (8.2) over the distant sidelobes be negligible compared to the corresponding integral over the first few lobes.

(Here it is assumed that in all directions, the distance across the array is of the same order of magnitude, namely L.) Equation (3.20) is the criterion for a well-filled array. In this case the distant sidelobes are expected to decrease with angular displacement almost as fast as for the aperture itself.

On the other hand, a *sparse* array is defined by the condition

$$N\lambda_c^2 / S_{\text{ap}} << 1 \tag{3.21}$$

For a sparse array, the first few angular sidelobes will still be given accurately provided that N is large enough compared to one.

3.2.3 Shaded Arrays

In Section 3.2.2 we paid particular attention to the case where there is no element shading of any kind. Three cases, each of which involves some kind of element shading, are discussed in Appendix A. The three cases turn out to be equivalent in their effect on $\overline{A}_0(\mathbf{r})$. Indeed the effect of each is equivalent to suitably modifying the 'shading' given by the smoothed-out element number density $\overline{g}(\mathbf{R})$ away from the value it has in the completely unshaded case. The theory of Sections 3.2.1 and 3.2.2 (in particular, Eqn 3.18) which *prima facie* applies only to the first two cases, applies also the third case with a trivial modification.

3.2.4 Directivity

$D(\theta,\phi;\theta_0,\phi_0)$, alternatively written $D(u,v;u_0,v_0)$, is *the far-field directivity of the smoothed aperture* $\overline{g}(\mathbf{R})$, for a target placed in the direction (θ_0,ϕ_0). (Note that this D incorporates any weighting factor $w(\mathbf{R})$, but does not incorporate the directivity of the individual elements). $D(\theta,\phi;\theta_0,\phi_0)$ is normalised so that $D(\theta_0,\phi_0;\theta_0,\phi_0)=1$. We therefore have $D(\theta,\phi;\theta_0,\phi_0)=\overline{A}_0(\mathbf{r})/\overline{A}_0(\mathbf{r}_0)$, where $\mathbf{r}=(r,\theta,\phi)$ is taken on the sphere $r=r_0$. Both numerator and denominator can be written out using the smoothed version of Equation (3.8). In the denominator, we have, from the normalisation (2.8),

$$\int w(\mathbf{R})\overline{g}(\mathbf{R})d^2R = \sum_n w_n = N \tag{3.22}$$

We therefore have, using (3.13),

$$D(\theta,\phi;\theta_0,\phi_0) = N^{-1}\int \exp[-j2\pi\boldsymbol{\kappa}_2\cdot\mathbf{R}]w(\mathbf{R})\overline{g}(\mathbf{R})d^2R \tag{3.23}$$

or equivalently (see Eqns 3.8, 3.12),

$$D(\theta,\phi;\theta_0,\phi_0) = N^{-1}\overline{G}^w(\boldsymbol{\kappa}_2) \tag{3.24}$$

Consider the directivity for a target at broadside, $D(\theta,\phi)$, defined by

$$D(\theta,\phi)=D(u,v)=D(u,v;0,0)=D(\theta,\phi;0,\varepsilon) \tag{3.25}$$

where the value of ε is arbitrary. Define

$$\boldsymbol{\kappa}_1=\lambda^{-1}(u,v) \tag{3.26}$$

Then we have, from (3.24), (3.15) and the definitions (3.25) and (3.26),

$$D(\theta,\phi)=N^{-1}\,\overline{G}^{w}(\boldsymbol{\kappa}_1) \tag{3.27}$$

From (3.23) and (3.15), $D(u,v;u_0,v_0)$ depends on its four arguments only through the differences $u-u_0$ and $v-v_0$; therefore

$$D(u,v;u_0,v_0)=D(u-u_0,v-v_0) \tag{3.28}$$

Note that the PSFs (3.12) and (3.18) likewise depend on the four directional coordinates only through $u-u_0$ and $v-v_0$.

The results (3.23) and (3.28) are of course not new; they pertain to the far field. What is new is that these same directivities pertain also to the near field, since (3.18) and (3.27) show that, on the sphere $r=r_0$,

$$\overline{A}_0(\mathbf{r})=ND_r a_0 H\,\overline{\sigma}\,D(u-u_0,v-v_0) \tag{3.29}$$

The conditions on this result, and likewise on the 'fundamental' result (3.18), consist of three requirements as follows:

(i) the image point lies on (or very near) the sphere $r=r_0$;

(ii) the toneburst parameters satisfy (3.17) (For a more general ξ, this condition is replaced by $B<<f_c$, as discussed below.); and

(iii) conditions (i) to (iii) in (3.4) hold.[14]

We note here the changes that must be made in the key results, (3.18) and (3.29), when a more general signal ξ is used in place of a toneburst. The 'more general' ξ discussed has carrier frequency f_c and satisfies Equations (4.4) and (4.5). These specified changes will be obtained in Section 4 but they are stated here for completeness. First we deal with the

[14] Recall that Equation (3.4) gives the conditions for the far-field expression to be accurate. Condition (iv) is here dropped from (3.4) since the tighter condition $r=r_0$ has already been imposed.

changes in the results themselves: essentially[15] the changes consist of simply replacing f throughout by f_c and λ by $\lambda_c = c/f_c$. Second, we deal with the conditions of validity, i.e. we specify the changes in the three conditions, (i) to (iii), on (3.18) and (3.29). Conditions (i) and (iii) are unaltered. Condition (ii) is replaced[16] by $B << f_c$, where B is the bandwidth.

For future use, we evaluate the integral of the squared directivity:

$$\begin{aligned}\int\left|D(u-u_0, v-v_0)\right|^2 du\,dv &= \int\left|D(u,v)\right|^2 du\,dv \\ &= N^{-2}\int\left|\overline{G}^w(\boldsymbol{\kappa}_2)\right|^2 du\,dv \\ &= \lambda_c^2 N^{-2}\int\left|\overline{G}^w(\boldsymbol{\kappa}_2)\right|^2 d^2\kappa_2\end{aligned} \tag{3.30}$$

Here, in the obtaining of the second and third lines, (3.27) and (3.15) have been used. (The mathematics of the 'element' $du\,dv$ in Equation 3.30 is discussed in Appendix B.) Parseval's theorem (equality of the 'energy' integral in the Fourier-transformed space and in the non-transformed space) then yields

$$\int\left|D(u-u_0, v-v_0)\right|^2 du\,dv = \lambda_c^2 N^{-2}\int\left[\overline{g}^w(\mathbf{R})\right]^2 d^2R \tag{3.31}$$

(absolute value signs being removed on the right-hand side of Eqn 3.31, since $\overline{g}(\mathbf{R})$ and $w(\mathbf{R})$ are real). For the case where there is no shading of any kind (i.e. $\overline{g}(\mathbf{R})$ and $w(\mathbf{R})$ uniform within the aperture), from (3.19), Equation (3.31) becomes

$$\int\left|D(u-u_0, v-v_0)\right|^2 du\,dv = \lambda_c^2/S_{\text{ap}} \tag{3.32}$$

Equation (3.31) may be written in another way by introducing a *shading correction factor* Q: this alternative form is described in Appendix B.

---

[15] Some of the replacements to be made in (3.18) and (3.29) are implicit rather than explicit. Thus replacements are to be made in Equations (3.13) and (3.15) that support Equation (3.18); and the directivity to be used in (3.29) is to be evaluated at f_c.

[16] This is also a *necessary* condition, since only then will the directivity $D(\theta,\phi)$ be essentially the same (having essentially the same first few nodes) for all Fourier components of $\xi(t)$.

3.3 Two Special Apertures

We mention two special apertures for which the directivity, given by (3.27), or by (3.23) with $\boldsymbol{\kappa}_1$ in place of $\boldsymbol{\kappa}_2$, comes out to a fairly simple expression. In both, the array is centred on the transmitter. The first is the circular aperture (uniform and unweighted, i.e. no shading of any kind) of diameter D. The directivity is

$$D(\theta,\phi) = 2J_1(x)/x \tag{3.33}$$

where J_1 is a Bessel function and

$$x = \frac{\pi D \sin\theta}{\lambda} = \frac{\pi D}{\lambda}\sqrt{u^2+v^2} \tag{3.34}$$

as given for example by Clay and Medwin [1977, p. 144], Ziomek [1985, p. 80] and Urick [1983, p. 59].

The second is the rectangular aperture (uniform and unweighted) having dimensions in the x and y directions equal to L_x and L_y respectively. The directivity [Clay and Medwin 1977, p. 144; Ziomek 1985, p. 74] is

$$D(u,v) = \operatorname{sinc}\left(\frac{L_x u}{\lambda}\right)\operatorname{sinc}\left(\frac{L_y v}{\lambda}\right) \tag{3.35}$$

where $\operatorname{sinc} x = \sin(\pi x)/\pi x$. From (3.33) and (3.35), the respective PSFs on the sphere through the point target can immediately be written down using (3.29).

4. The Three-Dimensional Point Spread Function

We now turn to the case where $\mathbf{r}$ is displaced in an arbitrary direction from the position $\mathbf{r}_0$ of the point target: the displacement has a component in the range direction as well as in the angular directions.

4.1 Calculation under Special Conditions

As an introduction for the reader that finds a concrete example illuminating, we first do the calculation for a special case involving a circular aperture.[17] The special case is specified as follows: (i) the signal is a toneburst (short, uncorrelated) given by (3.6); (ii) the receiver is an aperture that is circular, of diameter D, centred on the transmitter, and unshaded; and (iii) the target is at broadside. The calculation itself is given in Appendix C.

[17] The reader is however warned that the calculation turns out to be at least as lengthy as that for the general case, given in Section 4.2.

The result for the point spread function is

$$\overline{A}_0(\mathbf{r}) = ND_r\overline{\sigma}a_0 H \exp\left[j4\pi\frac{1}{\lambda}(r-r_0)\right]\mathrm{rect}\left[\frac{2(r-r_0)}{cT}\right]\frac{2J_1(x)}{x} \tag{4.1}$$

where x is given by (3.34). In (4.1) the overbar on $A_0(\mathbf{r})$ is actually not necessary—for an aperture. However by inserting the overbar we obtain a result that is valid also for a circular *array* provided that it is unshaded in any way. The conditions on the result (4.1) are those already imposed in Sections 2 and 3 (together with (i) to (iii) in the paragraph above).

Note that the result (4.1) may be rewritten as

$$\overline{A}_0(\mathbf{r}) = ND_r\overline{\sigma}a_0 H\,\xi\left[\frac{2}{c}(r-r_0)\right]D(u-u_0, v-v_0) \tag{4.2}$$

from (3.6) and (3.33). We shall find that this result, obtained subject to the restrictions (i), (ii) and (iii), holds much more generally.

4.2 Calculation for General Case

We now give a treatment paralleling that of Section 4.1 but without making any of the assumptions (i) to (iii). In particular, we consider a more general signal $\xi(t)$. As a preliminary, for a general signal $\xi(t)$ (uncorrelated, i.e. short pulse), we define the *effective pulse length* as

$$T_e = \int|\xi(t)|^2\,dt \tag{4.3}$$

The normalisation of ξ, given below (2.2), makes this definition reasonable. Note that the definition agrees with the actual pulse length T in the case of a rectangular pulse (3.6).

The more general ξ that we consider is a sinusoid (carrier frequency f_c) multiplied by a slowly-varying envelope. Specifically, let

$$\xi(t) = \xi_v(t)e^{j2\pi f_c t} \tag{4.4}$$

where $\xi_v(t)$, the complex envelope, is taken to have almost all of its energy contained in frequency components that satisfy

$$f \lesssim 1/T_e \tag{4.5}$$

(Thus $\xi(t)$ itself has almost all of its energy concentrated in $|f-f_c| \lesssim 1/T_e$.) This is an important and relevant case; for example, it includes the linear chirp after dechirping (discussion of such decoded signals is however postponed to Section 5.3).

We now impose the condition

$$B << f_c \tag{4.6}$$

on the beamwidth B; we saw below (3.29) that this condition is required. In the sense (4.6) the signal is narrowband. Now the 'uncertainty principle' tells us that

$$BT_e \gtrsim 1$$

This equation entails that under the condition (4.6) we also have

$$f_c T_e >> 1 \tag{4.7}$$

We return to Equation (3.5), which continues to give the PSF in the 3-D case. In (3.5), we first replace the summation with an integral over $\mathbf{R}$ as in (3.8), but for the more general ξ (4.4). Then the term $-(\hat{r}-\hat{r}_0)\cdot\mathbf{R}$ occurring in the argument of ξ_v (but not in the carrier) may be dropped, for the following reason. Because $\mathbf{r}$ is within the first few angular sidelobes, this term is less than or of order λ_c, where $\lambda_c = c/f_c$. Thus in (3.5), the second term (after the removal of the square brackets) is less than or of order $1/f_c$. Recall that we imposed the condition (4.7) (indirectly). Then the reason why the second term can be dropped is that, in the time interval $1/f_c$, ξ_v cannot change significantly. This in turn is because, from (4.5), there are no Fourier components of sufficiently high frequency to produce a difference. This dropping of the second term is the generalisation of the dropping of the second term in E_3 that occurred in Section 4.1. Note that the condition (4.6) replaces the condition (3.17) in the case of the more general ξ.

The expression for $A_0(\mathbf{r})$ then reduces to

$$A_0(\mathbf{r}) = D_r a_0 H \bar{\sigma} \xi\left[\frac{2}{c}(r-r_0)\right] \int \exp\left[-j\frac{2\pi}{\lambda_c}(\hat{r}-\hat{r}_0)\cdot\mathbf{R}\right] w(\mathbf{R}) g(\mathbf{R}) d^2R \tag{4.8}$$

This is identical to the on-sphere (and toneburst) expression (3.8), except that (i) the factor $\xi[2(r-r_0)/c]$ has been inserted, and (ii) λ_c has replaced λ. Therefore the rest of the argument in Section 3.2 again applies. Consequently we may immediately generalise Equations (3.12), (3.18) and (3.29) for the PSF to the 3-D case. The latter two yield

$$\bar{A}_0(\mathbf{r}) = D_r a_0 H \bar{\sigma} \xi\left[\frac{2}{c}(r-r_0)\right] \bar{G}^w(\boldsymbol{\kappa}_2) \tag{4.9}$$

$$\bar{A}_0(\mathbf{r}) = N D_r a_0 H \bar{\sigma} \xi\left[\frac{2}{c}(r-r_0)\right] D(u-u_0, v-v_0) \tag{4.10}$$

where it is understood that κ_2 in (4.9), and D in (4.10), are to be evaluated at the carrier frequency f_c. All three restrictions at the start of Section 4.1 have been removed.

It is interesting that, under the rather general conditions considered, the image amplitude turns out to be *separable*: it is the product of a factor that depends only on the ranges and a factor that depends only on the angular coordinates.

The conditions on the results (4.9) and (4.10) consist of two only, as follows:

(i) the condition (4.6) on the bandwidth; and

(ii) the conditions (i) to (iv) in (3.4) (i.e the conditions for the 'far-field' expression or 'close-to-target' approximation to hold).

4.3 Conditions for 'Area under the Curve'

It is of interest to know the conditions under which the expressions (4.9) and (4.10) are accurate over a region that covers nearly all the 'area' under the curve of the PSF $\left|\overline{A}_0(\mathbf{r})\right|^2$ of the smoothed array, so that the integral over all space is given accurately. (Because the region is three-dimensional, the 'area' is actually a 4-D entity.) In respect of the integration over the angular coordinates, Equation (3.4)(i) ensures that the first few sidelobes are given accurately, and hence that the integral to infinity is given to a good approximation (for $\overline{A}_0$, not necessarily A_0). Therefore we need only consider the range direction. For that direction, from simple speed-of-sound considerations, (for a short pulse) the sidelobes extend over

$$|r - r_0| \lesssim cT_e$$

For a correct 'area,' it is required that this region lies within the region of validity (3.4)(iv). For r_0 in the near field ($r_0 \lesssim L^2/\lambda_c$), this implies that a sufficient condition is

$$cT_e << \lambda_c (r_0/L)^2$$

i.e.
$$1/T_e >> f_c (L/r_0)^2 \qquad (4.11)$$

For most waveforms used, the uncertainty principle $BT_e \gtrsim 1$ can be replaced by $BT_e \sim 1$, so the condition (4.11) takes the form[18]

---

[18] For the reflectivity experiment, we can be more precise. As discussed at (3.4), it appears that a more precise statement of (3.4)(iv)(a) is

$$|r - r_0| << \tfrac{7}{2}\lambda_c (r_0/L)^2$$

$$B >> f_c (L/r_0)^2 \tag{4.12}$$

For r_0 in the far field ($r_0 >> L^2/\lambda_c$), the condition (4.11) is replaced by

$$1/T_e \gtrsim c\lambda_c/L^2 \tag{4.13}$$

and the condition (4.12) is replaced by

$$B \gtrsim c\lambda_c/L^2 \tag{4.14}$$

The conditions for (4.9) and (4.10) to correctly give the 'area' are therefore threefold:

(i) condition (4.6);

(ii) conditions (i) to (iii) (not (iv)) in (3.4); and

(iii) condition (4.11), or (4.13) if r_0 is in the far field.

4.4 Inclination Effects

When the point target position $\mathbf{r}_0$ is changed from broadside to some other direction from the array, the point spread function varies in a simple way described below. The form of this variation is well known for the far field, but is repeated here because of its greater generality.

The reader is asked to think of the PSF as a graph of A_0^2 versus $\mathbf{r}$ at constant range $r = r_0$, that is, a graph versus θ and ϕ. The graph is therefore a surface; it has a strong peak at $\mathbf{r}_0$. From (4.10), the PSF has the *same peak value* as if the target were at broadside. However, the shape of the graph is altered. Because u and v are not *linearly* related to angle traversed, the graph is *stretched laterally in the direction of increasing* θ. In fact, from (3.14) and (4.10), the angular beamwidth becomes greater by a factor

$$1/\cos\theta_0$$

than at broadside. In the direction of increasing ϕ there is no stretching; the angular beamwidth in the ϕ direction is the same as at broadside. These results hold subject to the conditions applicable to (4.10) and stated at that point; note that the target need not be in the far field.

A chirp was used. As will be shown in Section 5.3, it is appropriate to consider, in place of $\xi(t)$, the chirp *after dechirping*. The envelope of the latter approximates to a sinc function and it is readily shown that the value of $|r - r_0|$ at half peak intensity of the image is about

$$|r - r_0| = c/4B$$

These last two equations imply that (4.12) should be replaced by

$$B >> \tfrac{1}{14} f_c (L/r_0)^2$$

In the reflectivity experiment, the latter condition in fact holds.

As is known from the far field, these results can be interpreted by saying that the array may be replaced by its projection onto a plane perpendicular to the radius vector to the target point.

5. Extensions of the Model

The experimental arrangement in the reflectivity experiment differs from the 'restricted basic model' of Section 2.2 in three ways.[19] To deal with the arrangement, the following three restrictions must be removed: (i) the use of a transmitter that lies in the plane of the array; (ii) the use of a point transmitter; and (iii) the restriction to a non-correlated signal. This work is done in the present section, resulting in expressions for the voltage streams and the point spread function that hold more generally. This work lays the foundation for Section 8.5, where it is shown that the integral relationship, if it holds for the model of Section 2.2, also holds when the three extensions are made. The latter result is necessary in order for the experiment to be analysed by the proposed method.

5.1 Transmitter Not in the Receiver Array Plane

We now deal with a (point) transmitter located away from the plane of the receiver array. We again require the transmitter to be fairly close to the array; specifically, we again impose the condition (2.9), where $\mathbf{r}_c - \mathbf{r}_t$ is now a 3-D vector. We develop the theory of this more general situation up to a certain point. We then make a comparison with the situation—already treated in Sections 2 to 4—in which the transmitter is moved to coincide with the array centre (i.e. the situation $\mathbf{r}_t = \mathbf{r}_c$). The comparison shows that 'little has changed.'

For convenience we make a comparison between the situation 'transmitter at any location' (to be represented by the super- or subscript TAany) and the situation 'transmitter at centre of array' (represented by TACA). If displacement from the centre of the array is found to make no difference to the results of interest, then our proof is complete: the choice of the *centre* as the reference state is only for convenience. The details of the derivation and comparison are given in Appendix D. The comparison leads (subject to certain conditions) to two main results. The first main result is that the two voltage streams are related by

$$E_n^{\mathrm{TAany}}(t) = E_n^{\mathrm{TACA}}\left[t - c^{-1}\left(|\mathbf{r}_0 - \mathbf{r}_t| - |\mathbf{r}_0 - \mathbf{r}_c|\right)\right] \tag{5.1}$$

Thus the displacement of the transmitter produces no other effect on the voltage stream $E_n(t)$ than a time shift. Furthermore this time shift is independent of n.

The second main result is that the two PSFs are related by

[19] This is apart from the possibility that the target may not be adequately represented by a collection of point scatterers.

$$\left[\overline{A}_0(\mathbf{r})\right]_{\text{TAany}} = \left[\overline{A}_0(\mathbf{r})\right]_{\text{TACA}} \times e^{j\phi} \tag{5.2}$$

where ϕ is real. *Thus the intensity PSF* $\left|\overline{A}_0(\mathbf{r})\right|^2$ *is unchanged by the displacement of the transmitter.*

The conditions required for the two main results are given in Appendix D. Of these conditions, Equation (D.12) is the one of most interest.

Appendix D also estimates the magnitude of the phase shift ϕ introduced into $A_0(\mathbf{r})$.

5.2 Spherical Transmitter

Consider the effects of replacing a point transmitter (located at $\mathbf{r} = \mathbf{r}_t$) with a spherical transmitter having the same centre. Consider a point target at $\mathbf{r}_0$. Potentially the voltage stream $E_n(t)$ is altered in four ways. The first effect is through the numerator b in Equation (2.1). As discussed below (2.10), this factor has no effect provided that, when comparing a spherical transmitter to a point transmitter, we always compare two transmitters that have the same value of the product bp_0. It will be assumed that this is done when writing equations such as (5.6) below. Second, there is the correction term b in the denominator of (2.1), associated with spherical spreading. This may be ignored provided we impose

$$b << r_0 \tag{5.3}$$

Third, there is the b in the attenuation factor in (2.6). This occurrence of b can be ignored provided we impose

$$\tfrac{1}{2}\alpha b << 1 \tag{5.4}$$

This condition is similar to the second condition imposed at (2.15). Fourth, there is the b in the argument of p_{trax} in Equation (2.6), reflecting the travel time across the radius. Of the four effects, this one alone survives. Thus the term $+b/c$ must be inserted into the argument of ξ. For an arbitrary origin, from (2.11) or (D.3), we therefore have for the voltage stream

$$E_n(t) = D_r a_0 H \sigma_n \xi\left[t - c^{-1}\left(|\mathbf{r}_0 - \mathbf{r}_t| + |\mathbf{r}_0 - \mathbf{r}_n| - b\right)\right] \tag{5.5}$$

Thus we have

$$E_n^{\text{ST}}(t) = E_n^{\text{PT}}\left(t + c^{-1}b\right) \tag{5.6}$$

Here ST and PT refer to the spherical transmitter and point transmitter respectively (both centred at $\mathbf{r}_t$).

When the image is formed via Equation (2.7), the term b introduced there exactly cancels that in (5.6), with the result that

$$A_0^{\mathrm{ST}}(\mathbf{r}) = A_0^{\mathrm{PT}}(\mathbf{r}) \tag{5.7}$$

Thus the two images of a point target are the same.[20]

Furthermore, due to superposition, the results (5.6) and (5.7) also hold for a *collection* of point targets (in which case Eqn 5.7 would of course be written without the zero subscripts).

5.3 Correlated Signal

It is common, as in the reflectivity experiment, to use a coded or chirped signal. This implies that, in the signal processing, each voltage stream is crosscorrelated with a replica of the transmitted signal; the resulting voltage streams are used in place of the original ones in image-forming. Let us take the dechirped voltage to be

$$E_n^{\mathrm{cor}}(t) = \frac{\int \xi^*(t') E_n(t'+t)\,dt'}{\int |\xi(t')|^2\,dt'} \tag{5.8}$$

Then, due to the linearity of the system, $E_n^{\mathrm{cor}}(t)$ is the voltage that would have been obtained had the initial normalised signal been, not $\xi(t)$, but

$$Y(t) = \frac{\int \xi^*(t') \xi(t'+t)\,dt'}{\int |\xi(t')|^2\,dt'} \tag{5.9}$$

That is, it is just as though the transmitted pressure in (2.2) had been $p_0 Y(t)$. *Results for all derived quantities can be made correct for a correlated signal by replacing* ξ *by* Y. Thus we have

$$\begin{aligned} E_n^{\mathrm{cor}}(t) &= \left[E_n^u(t) \text{ in terms of } \xi\right]_{\xi \to Y} \\ A^{\mathrm{cor}}(\mathbf{r}) &= \left[A^u(\mathbf{r}) \text{ in terms of } \xi\right]_{\xi \to Y} \end{aligned} \tag{5.10}$$

Here cor means 'after crosscorrelation,' while u (for uncorrelated) means 'calculated without crosscorrelation.' The subscript $\xi \to Y$ means that ξ is to be replaced by Y. These results apply even for complex targets. For a point target, the square brackets in (5.10) are given by (2.11) and (2.16) respectively (for a point transmitter at the array centre). Note that $Y(t)$ is

---

[20] This holds provided that the two transmitters being compared are at the same point (same centre). If we compare with a transmitter at the array centre, then, as Section 5.1 shows, we are limited to saying that the absolute values of the image amplitudes are equal.

normalised in the same way as $\xi(t)$, since (i) $Y(0)=1$ and (ii) the latter is the maximum value achieved by $|Y(t)|$ (compare Eqn 2.3 and the discussion at Eqn 2.2).

The *effective pulse length* of the correlated pulse is defined as

$$T_{er} = \int |Y(t)|^2 dt \tag{5.11}$$

and in practice is much shorter than T_e defined by (4.3). Concerning bandwidth, in the case of a correlated signal, we do not impose (4.5) as it stands. Instead, let

$$Y(t) = Y_v(t) e^{i2\pi f_c t} \tag{5.12}$$

Then we take $Y_v(t)$, the complex envelope of $Y(t)$, to have almost all its energy contained in frequency components that satisfy

$$f \lesssim 1/T_{er} \tag{5.13}$$

In summary, in any result for uncorrelated signals that contains $\xi(t)$, $\xi_v(t)$ or T_e, those quantities should be replaced by $Y(t)$, $Y_v(t)$ and T_{er} respectively, in order for the result to apply to correlated signals.

Clearly the procedures of Sections 5.1, 5.2 and 5.3 may be combined to yield the modified PSF in the case where the transmitter is not at the array centre or even in the array plane, the transmitter is a sphere rather than a point, while at the same time the signal may be correlated.

6. Image of a Small, Smooth Ball

An understanding of the smooth ball target is needed for calibration in the reflectivity experiment. While some rather general theory is developed in this section, the results from it that are needed for the experiment are twofold. First, under a certain condition, given by Equation (6.15) below, the ball may be treated as a point scatterer located on the ball's surface. The location of the point may be taken at any reasonably chosen 'centre' of the points of reflection of rays from the transmitter that go on to reach the array. The 'point scatterer' condition is satisfied in the experiment. The second result is that the equivalent point reflector has a target strength given by $a_0 = a/2$ (Eqn 6.18), where a is the radius of the ball. This relationship is in agreement with a well-known result.

The focus in Sections 6.1 and 6.2 is on developing equations describing the system of sonar plus ball under the principal condition $\lambda << a$. Section 6.1 treats reflection from the ball under this condition, which permits the use of geometrical acoustics. Section 6.2 brings in the rest of the measurement system—considerations of the pressure field and the

transducers. The treatment to the end of Section 6.2 is a 'non-point treatment,' referring to the fact that, while the condition $a << r_0$ is imposed at this stage, we do not yet restrict a to even lower values, as is required in order to treat the ball as a point. Section 6.3 imposes an appropriate further condition in order to justify the treatment of the ball as a point scatterer.

6.1 Reflection from the Ball: Geometrical Acoustics

Consider a spherical target of radius a. Under the short wavelength condition

$$\lambda << a \tag{6.1}$$

geometrical acoustics, i.e. a ray treatment, is valid.[21] The precise limitation on λ/a may be discerned from Morse and Ingard [1968, p. 419]. From their equation that follows (8.2.3), at large values of a/λ the total scattering cross section is $2\pi a^2$, where the difference from the geometrical cross section πa^2 is explained in Morse and Ingard. The graph in their Figure 4 suggests that this asymptotic value, $2\pi a^2$, is attained to a good approximation for $2\pi a/\lambda \geq 20$, i.e. for

$$\lambda/a \leq \pi/10 \tag{6.2}$$

We impose this condition and apply geometrical acoustics. In the reflectivity experiment $\lambda \approx 0.5\,\text{mm}$, so the geometrical acoustics condition on a is $a \geq 1.5\,\text{mm}$. Since $a \approx 5\,\text{mm}$, the condition is well satisfied.

The ball is assumed to have a high acoustic impedance relative to the water, so that to a good approximation all the incident energy is reflected. Then from geometrical acoustics we have that the incident and scattered acoustic intensities, I_{in} and I respectively, are related by

$$I = I_{\text{in}}\, a^2/4R^2 \tag{6.3}$$

the scattering being isotropic.[22] (Here I is measured at distance R from the centre of the ball). Strictly this result does not hold at finite distances R, since reflection occurs at the ball's surface, not at its centre. However Equation (6.3) will accurately represent intensity as a function of the scattering angle provided

$$R >> a \tag{6.4}$$

---

[21] This is true except near the forward direction—a complication that need not concern us (see Grandy [2000, pp. 33, 42]).

[22] Strictly speaking, geometrical acoustics does not tell the whole story. For the monofrequency case, when I is considered as a function of the scattering angle, superposed on the omnidirectional term in the intensity, i.e. the right-hand side of (6.3), is a rapidly fluctuating term of similar size that averages to zero [Morse and Ingard 1968, Eqn 8.1.4]. However, these fluctuations are removed if the spread of frequencies is sufficiently large. In the present experiment, it is estimated that the fluctuations are largely removed. We shall ignore the small correction due to the remaining fluctuations. In the 'energy conservation' relationship (8.3), it may be that the remaining fluctuations are equivalent to a small additional departure of the ratio $\overline{\sigma}/\sigma_{\text{rms}}$ from unity.

Let $\mathbf{r}_t$ and $\mathbf{r}_n$ be the locations of the transmitter centre (radius $= b$) and the nth element respectively. By tracing the appropriate ray, we now obtain the outward and return path lengths, r_{out} and $r_{\text{ret}} = r_{\text{ret}\,n}$ respectively, for a ray specified by $(\mathbf{r}_t, \mathbf{r}_n)$. Let

$$\mathbf{R}_t = \mathbf{r}_0 - \mathbf{r}_t \quad \text{and} \quad \mathbf{R}_r = \mathbf{r}_0 - \mathbf{r}_n \tag{6.5}$$

denote the vectors to the centre of the ball (at $\mathbf{r}_0$) from the transmitter centre and the receiver element respectively. Let $2\gamma_n$ be the angle between the vectors $\mathbf{R}_t$ and $\mathbf{R}_r$ (see Fig. 5). In accordance with (6.4) we impose the condition that the various ranges[23] are large compared to the radius a:

$$r_0 >> a \tag{6.6}$$

[23] Besides (6.6) it is understood that b, r_t and L are all small compared to r_0. The latter three conditions are introduced formally below (6.9).

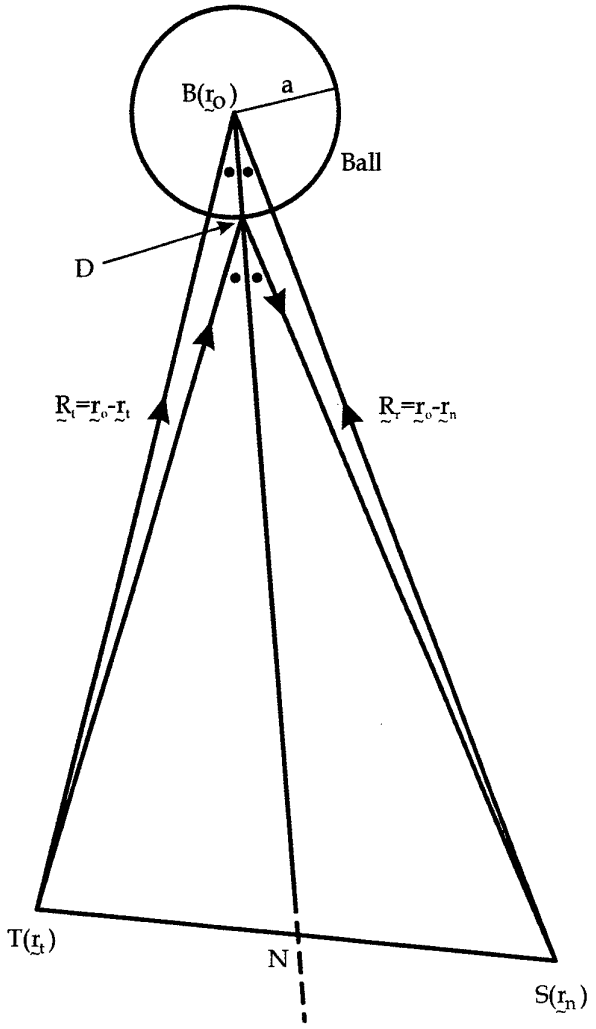

Figure 5: *Geometry for reflection from ball. T=spherical centre of transmitter. S=receiving element. Each of the four angles labelled with a dot equals γ_n, at least approximately, because the ball is small. The bisector BD passes extremely close to N, the midpoint of TS. Section 6.3 considers the special case where S is at $\mathbf{r}_c$, the centre of the array; then BD passes extremely close to $\frac{1}{2}(\mathbf{r}_t + \mathbf{r}_c)$.*

We first write a rather complex formula for the angle γ_n by applying the sine rule to the triangle formed by the transmitter centre, the element and the ball centre:

$$\frac{\sin 2\gamma_n}{|\mathbf{r}_n - \mathbf{r}_t|} = \frac{\sin(\mathbf{R}_t, \mathbf{r}_n - \mathbf{r}_t)}{R_r} = \frac{\sin(\mathbf{R}_r, \mathbf{r}_t - \mathbf{r}_n)}{R_t} \tag{6.7}$$

Here $(\mathbf{A},\mathbf{B})$ means the angle between the vectors **A** and **B**. This pair of equalities actually gives two expressions for $\sin 2\gamma_n$. The formula is exact; it does not rely on (6.6). It will be simplified below.

The path lengths can be shown to be

$$\begin{aligned} r_{\text{out}} &= R_t - b - a\cos\gamma_n + (a^2/2R_r)\sin^2\gamma_n + \cdots \\ r_{\text{ret}} &= R_r - a\cos\gamma_n + (a^2/2R_t)\sin^2\gamma_n + \cdots \end{aligned} \tag{6.8}$$

where our main interest will be in the terms up to and including the cosine. We now show how to derive that part of the two expansions. Subject to (6.6), the ray from the transmitter that is reflected to the receiver from the ball's *surface* may be assumed parallel to the line from the transmitter to the centre of the ball. It follows, by ray geometry, that (i) the angle of incidence of the ray that is reflected to the receiver element is γ_n; (ii) hence the angle of reflection is also γ_n; and (iii) the path lengths are given by the terms in (6.8) up to and including the cosine term.

For the more complete expansion (6.8), the derivation proceeds by writing down several equations for the exact geometry instead of invoking (6.6). Then, the solution for r_{out} and r_{ret} can be developed in ascending powers of a/R_t and a/R_r. The resulting expansion, to one 'extra' term, is (6.8).

6.2 The Ball in the Context of the Imaging System

We now combine the geometrical acoustics with considerations of the pressure field to obtain formulae which, in principle, give the voltage stream and the image amplitude. From (6.3), the complex pressures are related by $|p| = |p_{\text{in}}|\, a/2R$. By the same argument as used to derive Equation (2.5), we obtain, for the voltage produced at the nth element,

$$E_n(t) = D_r \sigma_n p_{\text{trax}}\left(t - \frac{r_{\text{out}}+r_{\text{ret}\,n}}{c}\right)\frac{bD_t}{r_{\text{out}}+b}\,\frac{a}{2r_{\text{ret}\,n}}\exp\left[-\frac{\alpha}{2}(r_{\text{out}}+r_{\text{ret}\,n})\right] \tag{6.9}$$

Here $D_{rn} = D_r$ has been assumed independent of n.

We allow the transmitter to be away from the array plane and the transmitter to be a sphere instead of a point. We note that certain approximations can be made, similar to those in Sections 2 and 5. Thus, first, we impose conditions on the attenuation coefficient α as follows: the two conditions in (D.1); the condition (D.2); and the condition (5.4). Second, we impose conditions concerned with spherical spreading as follows: $L << r_0$ (first equation in 2.14); $|\mathbf{r}_t - \mathbf{r}_c| \le \frac{3}{4}L$ (Eqn 2.9); and $b << r_0$ (Eqn 5.3). (Note that $a << r_0$ has already been imposed at Eqn 6.6). With the use also of (2.2), Equation (6.9) becomes

$$E_n(t) = D_r \sigma_n \frac{bp_0 D_t}{r_0^2}\,\frac{a}{2}\exp(-\alpha r_0)\,\xi\left[t - c^{-1}(r_{\text{out}}+r_{\text{ret}\,n})\right] \tag{6.10}$$

Here

$$r_{\text{out}} + r_{\text{ret}\,n} = |\mathbf{r}_0 - \mathbf{r}_t| + |\mathbf{r}_0 - \mathbf{r}_n| - b - 2a\cos\gamma_n \tag{6.11}$$

Under the conditions stated, the equation (6.7) giving γ_n may be simplified to

$$\frac{2\gamma_n}{|\mathbf{r}_n - \mathbf{r}_t|} = \frac{\sin(\mathbf{r}_0, \mathbf{r}_n - \mathbf{r}_t)}{r_0} \tag{6.12}$$

it being noted that $\sin 2\gamma_n \approx 2\gamma_n$ since γ_n is small.

Actually, while the sine-squared terms in (6.8) are small relative to r_0, or even relative to a, it is not necessarily valid to drop them. This is because, to drop them in a 'phase' context, we need them to be small on the scale of a *wavelength*. The test is as follows: when the expressions (6.8) are substituted into the argument of ξ in (6.10), the sum of the two sine-squared terms must be small compared to a quarter-wavelength at the central frequency, namely $\lambda_c/4$. The condition for this turns out to be

$$\frac{9}{4}\frac{a^2 L^2}{r_0^3} << \lambda_c \tag{6.13}$$

In the case of the reflectivity experiment, the ratio of the left- to the right-hand side comes out to be 4.4×10^{-4}, so that the condition is very easily satisfied.

We shall not proceed further with the mathematics of the 'general' or non-point case, except to point out the following feature of the ball reflector. A given element essentially receives its acoustic energy from one small region of the ball's surface—a different region for each element. Thus *there is a correlation between the element and the region* (say S) *of reflection.*

In the next section we shall specialise to the case in which the region S on the surface moves so little when we switch from one extreme sensor element to another that the sphere is equivalent to a point scatterer. In that case the above correlation disappears. It should be noted that Equations (6.10) to (6.12) are not restricted to this 'point scatterer' case, which requires a small radius satisfying condition (6.15) below. The Equations (6.10) to (6.12) apply to somewhat larger spheres, still satisfying $a << r_0$ but not requiring (6.15).

6.3 Treatment of Ball as a Point Scatterer

We derive the condition under which the sphere is equivalent to a point scatterer. Let T (at $\mathbf{r}_t$) be the location of the transmitter centre, C (at $\mathbf{r}_c$) be the central point of the receiving array, and let B (at $\mathbf{r}_0$) be the ball's centre. Note that the transmitter is allowed to be

anywhere subject to the conditions given in Section 5.1. Consider the point A that geometrically reflects the ray from the transmitter to C. To a sufficient approximation, the location of A may be written as[24]

$$\mathbf{r}_A = \mathbf{r}_0 + a\frac{(\mathbf{r}_c + \mathbf{r}_t)/2 - \mathbf{r}_0}{|(\mathbf{r}_c + \mathbf{r}_t)/2 - \mathbf{r}_0|} \tag{6.14}$$

Because the choice of this location A on the surface has been based on the central point of the array, it gives the best *single-point* representation of the sphere.

The condition under which a point target at this location is an adequate representation of the sphere is found in Appendix E. The condition comes out to be

$$\tfrac{1}{4}a(L/r_0)^2 << \lambda_c \tag{6.15}$$

Here L is the maximum dimension of the array (measured diagonally in the case of a rectangular array).[25]

It is of interest to compare (6.15) with the condition $a << r_0$ already imposed at Equation (6.6). Provided the ball is in the near field (in the sense $r_0 << L^2/\lambda_c$, i.e. with no dependence on the angle θ_0 of the ball away from broadside), the new condition (6.15), which may be rewritten as

$$a << r_0 \frac{4r_0}{L^2/\lambda_c}$$

is more restrictive than the old condition $a << r_0$. Thus the making of the point scattering approximation requires the ball to be *smaller* (i.e. smaller than $a << r_0$ requires).

In the reflectivity experiment, near-field conditions apply. Also, in (6.15,) the ratio of the left-hand side to the right-hand side comes out to be 0.11, so that the condition (6.15) for the point scatterer treatment is satisfied.

We proceed to obtain the expression for the voltage stream $E_n(t)$. We may take the path to be always via A, so that in (6.10),

---

[24] To obtain (6.14), note that the coefficient of a is a unit vector. An exact equation would have here a vector lying along the line BAP through B and A that bisects the angle TAC. Because the angle TAC is small, to a good approximation BAP passes through the point $\frac{1}{2}(\mathbf{r}_t + \mathbf{r}_c)$; whence the result.

[25] In the case of a non-broadside location combined with an array that has two characteristic lengths (L_x and L_y say), it may be possible to replace (6.15) by a somewhat weaker condition.

$$r_{\text{out}} + r_{\text{ret}\,n} = |\mathbf{r}_A - \mathbf{r}_t| - b + |\mathbf{r}_A - \mathbf{r}_n| \tag{6.16}$$

The result for $E_n(t)$ for the ball is thus given by substituting (6.16) into (6.10). Now compare this with the result for $E_n(t)$ for a *point* target, given[26] by substituting (2.13) into (5.5). The expressions differ only in two respects. First, $\mathbf{r}_A$ replaces the general point target location as expected. Second, $a/2$ replaces a_0. Thus the equivalent target strength of the sphere of radius a is

$$a_0 = a/2 \tag{6.17}$$

This result agrees with the usual result for the target strength of a sphere (Urick 1983, p. 303).

We have found that, under stated conditions, the ball is equivalent to a point target with the position and target strength as stated. It follows that the image $A(\mathbf{r})$ is centred at A and is the same as for a point target of strength $a_0 = a/2$.

Note that, if we choose the origin at $\frac{1}{2}(\mathbf{r}_t + \mathbf{r}_c)$, then the position of A, given by Equation (6.14), simplifies to

$$\mathbf{r}_A = (r_0 - a)\hat{\mathbf{r}}_0 \tag{6.18}$$

7. Image of a Rough, Flat Surface

7.1 Incoherent Scattering from a Surface

We define four quantities for acoustics by analogy with optics, in particular, radiometry. (For the optical/radiometric definitions, refer to Williams[27] [1970, p. 22] or Jerlov [1976, pp. 4, 9].) In this report, in the absence of any better names on offer, the relevant *acoustic* quantities are denoted by the *optical* terms (e.g. 'radiant flux'), but placed in inverted commas.[28] For the symbol of an acoustic quantity, the standard optical symbol is used, but with a prime added to signify the acoustic quantity (e.g. F' for 'radiant flux').

The quantities are as follows.

---

[26] The origin is arbitrary for both results for $E_n(t)$.

[27] Regarding radiance, the reader should ignore Figure 9 of Williams; for corroboration of this statement, see Jerlov [1976] or another text.

[28] Note that in this report there is no weighting of the quantities according to the sensitivity of the ear or the eye, such as occurs in photometry.

- *'Radiant flux'* F' is acoustic power (in watts). Usually it is the power crossing some area.
- *'Radiant intensity'* I' is the acoustic power emitted by a source, or by an element of a source, per unit solid angle (unit: $\mathrm{W\,sr^{-1}}$). In general it depends on the direction from the source to the point of observation (directional source).
- *'Irradiance'* E' is the acoustic power received per unit area of the surface being ensonified (unit: $\mathrm{W\,m^{-2}}$). Note that the area is of the element of surface itself; there is no projection onto a surface at right angles to the direction of energy flow.
- Given a surface that reflects or emits sound, the *'radiance'* L' received *at* a point *from* a point on the surface is defined thus: L' is the acoustic power received per unit solid angle from unit *projected* area of the surface. The projection is onto a plane at right angles to the line joining the one point to the other (direction of flow).[29] The unit of L' is $\mathrm{W\,m^{-2}\,sr^{-1}}$.

We also introduce the usual *acoustic intensity*, denoted by I (without a prime). I is a vector with its direction in the direction of energy flow. Its magnitude is the power crossing unit area, where that area is at right angles to the direction of energy flow [Morse and Ingard 1968, p. 249].

By definition, a *uniformly diffusing surface* is a surface for which, no matter from which direction it is ensonified, the 'radiance' of the surface (due to the reflected radiation) is the same in all directions. We shall refer to a surface as *'white'*, or acoustically white, if it is uniformly diffusing and it reflects *all* the acoustic energy that falls on it (thus no energy is absorbed or transmitted). As shown in the text by Longhurst [1957], the total 'radiant flux' radiated by a uniformly diffusing surface element dS is given in terms of the 'radiance' L' of the surface element by

$$dF' = \pi L' dS \tag{7.1}$$

Now suppose an acoustic intensity I_{in} falls upon a 'white', flat surface of area S, with angle of incidence i. Then the 'radiant flux' reaching the surface is

$$F'_{\mathrm{in}} = I_{\mathrm{in}} S \cos i \tag{7.2}$$

---

[29] The 'radiant flux' from an element of surface dA into an element of solid angle $d\Omega$ may be written as

$$dF' = L' dS\, d\Omega$$

where $dS = dA\cos\theta$ is an element of projected area. The existence of two independent elements, dA and $d\Omega$, can cause confusion, connected with the question of which of these two elements is to be made to approach zero the fastest. Here one should think of the element of area dA as *very* small, and the element of solid angle $d\Omega$ as merely small. By this we mean that dA is to be so small as to be pointlike in comparison with the spherical cap of a 'cone' opening out at $d\Omega$ from dA and capped at the point of observation.

The 'radiant flux' *reflected* from S may, from (7.1), be written in terms of the 'radiance' L' by $F' = \pi L' S$. Also, since the surface is 'white,' we have $F' = F'_{\text{in}}$. These last two equations may be combined with (7.2) to yield for the 'radiance'

$$L' = \pi^{-1} I_{\text{in}} \cos i \tag{7.3}$$

For an acoustic system, the reflection coefficient of a surface [Meyer and Neumann 1972] is defined as the fraction of the incident sound energy that is reflected. This definition is not adequate in the angle-dependent case. We now generalise to this case. Let the incoming sound have angle of incidence i. After reflection, consider the 'radiance' $L'(R, g)$ produced in a particular direction, to be called the direction of the reflected ray. This direction may be specified by two angles: (i) the angle of reflection R, and (ii) the angle between the plane of incidence and the plane of reflection,[30] to be called g. Then we define the *reflection coefficient* $\rho(i, R, g)$ as the extra factor that must be inserted into the right-hand side of (7.3) to convert the 'radiance' of a 'white' surface into the actual 'radiance':

$$L'(R, g) = \pi^{-1} I_{\text{in}} \rho(i, R, g) \cos i \tag{7.4}$$

Note that (7.4) enables us to distinguish between 'diffuse' reflection (ρ having a wide spread over R and g) and 'specular' reflection (ρ being sharply peaked in R and g).

From the definitions we note that, for the reflected beam in the direction (R, g) at distance r, the 'radiant flux' through an element of solid angle $d\Omega$ is

$$F' = L' S \cos R \, d\Omega$$

provided that r is large compared to the linear size of the reflecting surface. But this 'radiant flux' is also related to the acoustic intensity I by

$$F' = I r^2 d\Omega$$

Therefore the acoustic intensity is given by

$$I = \frac{L'}{r^2} S \cos R \, ; \tag{7.5}$$

and so, from (7.4),

---

[30] The angle of reflection is the angle between the reflected ray and the normal to the surface. The plane of reflection is the plane containing both the reflected ray and the normal.

$$I = \frac{1}{\pi}\frac{I_{\text{in}}}{r^2} S \rho \cos i \cos R \tag{7.6}$$

The key equation (7.4) defining the reflection coefficient is based on energy flows only and ignores the phase of the acoustic wave. The concept of energy flows combining incoherently will be used explicitly in Section 7.2. (This happens at Eqn 7.15, where the intensities $|\xi_v|^2$ are combined without regard to phase.) Yet for a perfect specular reflector, the reflected rays have definite phase relationships with each other. This raises the question of whether, as the surface approaches the condition of perfect specularity, the treatment breaks down, due to the collection of waves having coherence properties. We have not been able to settle this question one way or the other, and leave it as an open question. The present treatment will be based on Equation (7.4).

7.2 Scattering in the Context of the Imaging System

We consider a small, flat target satisfying the model of Section 7.1 and forming part of the imaging system of the basic model (Section 2). We first write I, the reflected acoustic intensity measured at the receiving array, in terms of I'_{trax}, the 'radiant intensity' emitted at the transmitter surface along the axis of the beam pattern. Let D_t, α, r_{out} and r_{ret} be defined as in Section 2.1, r_{out} now being measured to the centre of the reflecting surface, and r_{ret} being measured from that centre to the centre of the receiving array. Then from the definitions, the acoustic intensity received at the target is

$$I_{\text{in}} = \frac{I'_{\text{trax}} D_t^2}{r_{\text{out}}^2} \exp(-\alpha r_{\text{out}}) \tag{7.7}$$

where D_t is evaluated in the direction of the centre of the target. Here attenuation has been taken into account. Here and below, the approximations made in Section 2.2 are again made, the conditions of validity being as before.

On the reflected side, I is given by an equation slightly modified from (7.6):

$$I = \frac{1}{\pi}\frac{I_{\text{in}}}{r_{\text{ret}}^2} S \rho \cos i \cos R \exp(-\alpha r_{\text{ret}}) \tag{7.8}$$

(see Fig. 6 below). Combining this with (7.7), we obtain

$$I = \frac{1}{\pi}\frac{I'_{\text{trax}} D_t^2}{r_{\text{out}}^2 r_{\text{ret}}^2} S \rho \cos i \cos R \exp[-\alpha(r_{\text{out}} + r_{\text{ret}})] \tag{7.9}$$

For Equations (7.7) to (7.9) to be valid, we require

$$M << r_{\text{out}}, \qquad M << r_{\text{ret}} \quad \text{and} \quad L << r_{\text{ret}} \tag{7.10}$$

Here M and L are the maximum dimensions of the target and array respectively. These conditions ensure the constancy of the incident acoustic intensity and angle of incidence over the target, and similarly for the reflected beam.[31]

We now relate I and I'_{trax} to pressure, and hence also to the voltage stream $E_n(t)$. As a result, as in Section 2, we relate $E_n(t)$ to the pressure at the transmitter. First, in a general travelling wave we have for the acoustic intensity

$$I = |p|^2 / 2Z \tag{7.11}$$

where Z is the acoustic impedance. The factor 2 arises because $p = p(t)$ in (7.11) is the analytic signal. Here I is taken to be the acoustic intensity averaged over one cycle. Hence, in the context of the signal $\xi(t)$, I is still time-dependent, but on a time-scale large compared to $1/f_c$.

We first apply (7.11) at the transmitter. From (2.2) and the fact that $I'_{\text{trax}} = b^2 I_{\text{trax}}$ (I_{trax} being the acoustic intensity measured at the surface of the transmitter on the axis), we have

$$I'_{\text{trax}}(t) = (2Z)^{-1} p_0^2 b^2 |\xi(t)|^2 \tag{7.12}$$

We now deal with the nth receiving element. We have, from (2.4) and (7.11),

$$|E_n(t)|^2 = 2Z D_r^2 \sigma_n^2 I(t) \tag{7.13}$$

At this stage we must recognise that in nonsteady conditions (such as in the reflectivity experiment), a time-delay must be incorporated onto Equation (7.9). Consider first the case where both the surface S and the array are pointlike, so that the travel times are unique. Then in (7.9), I and I'_{trax} should be written as

$$I(t), \qquad I'_{\text{trax}}\left[t - c^{-1}(r_{\text{out}} + r_{\text{ret}})\right]$$

---

[31] Regarding these constancies, see also: (i) the comments below (I.1), including the footnote, and (ii) the text at Equation (I.4).

respectively. With this understanding, when (7.12) is substituted into (7.9) and the result into (7.13), one obtains, for a surface characterised by a reflection coefficient $\rho(i,R,g)$:

$$|E_n(t)|^2 = (D_r\sigma_n H)^2\pi^{-1}S\rho\cos i\cos R\left|\xi_v\left[t-c^{-1}\left(r_{\text{out}}+r_{\text{ret}}\right)\right]\right|^2 \tag{7.14}$$

Here H is given by (2.13) and Equation (4.4) has been used to replace ξ by ξ_v.

Up to now it has appeared that we may take account of the nonzero size of the flat reflecting surface by simply replacing dS by S. However the introduction of a time-dependent signal of amplitude ξ_v means that signals of different amplitude may be reaching different parts of the surface at the same time. In that case, Equation (7.14) requires modification as follows. In the delay, in (7.14), $r_{\text{out}}+r_{\text{ret}}$ is replaced by

$$r_{\text{out}\,S}+r_{\text{ret}\,S,n}$$

where, for example, the return path depends both on n and on the position of the point of reflection on the surface, this position being formally represented by S. Then in place of (7.14) we get

$$|E_n(t)|^2 = (D_r\sigma_n H)^2\pi^{-1}\int\rho\cos i\cos R\left|\xi_v\left[t-c^{-1}\left(r_{\text{out}\,S}+r_{\text{ret}\,S,n}\right)\right]\right|^2 dS \tag{7.15}$$

Here the main purpose in writing the result as an integral has been to deal with the time dependence. However at the same time, let us choose (if only temporarily) to make the formula (7.15) more accurate by allowing i, R and $\rho=\rho(i,R,g)$ to depend on both[32] S and n.

In Section 8.7, the summed integral of (7.15), which is relevant to the integral relationship and to the analysis of the experiment, will be evaluated, subject to certain approximations.

[32] The conditions of validity given by (7.10) are still required however, so that the spherical spreading factors may be taken as constant over the target and also over the receiving array. This prompts the question: Why bother taking account of the dependence of ρ on S, when the condition of validity for taking $\rho=\text{const.}$ is also Equation (7.10)? The answer is that the error in the 'ρ' approximation depends also on the shape of the 'curve' $\rho(i,R,g)$. As a result, the relative error in the 'ρ' approximation is sometimes far greater than the relative error in taking the spreading factor to be constant.

8. The Proposed Integral Relationship

8.1 Overview

For any target (not necessarily a point), the image amplitude $A(\mathbf{r})$ is determined by the received voltage streams $E_n(t)$ according to Equation (2.7). Consider the following two integral expressions:

$$J_a = \int \sum_n w_n^2 |E_n(t)|^2 dt \tag{8.1}$$

$$J_i = \int \left|\overline{A}(\mathbf{r})\right|^2 \frac{\cos\theta}{r^2} d^3r \tag{8.2}$$

In (8.1), the integral is over all times at which returns from the transmitted pulse concerned are being received. In (8.2), θ is measured from broadside. As discussed in Section 3.2.2, the writing of $\overline{A}$ in place of A effectively means that the contributions of distant sidelobes in $A(\mathbf{r})$ are to be ignored. It is conjectured that the ratio J_i/J_a is a 'constant,' independent of 'almost everything.' The value of the constant is found in Appendix F, in which, for the special case of a *point* target in the restricted basic, or unextended, model of Section 2.2: (i) it is shown that J_i/J_a is indeed a constant, and (ii) the value of the constant is found to be the right-hand side of (8.3). Inserting that value, we have as the conjectured *general* relationship,

$$\frac{J_i}{J_a} = \frac{c}{2}\left(\frac{\overline{\sigma}}{\sigma_{\text{rms}}}\right)^2 \lambda_c^2 \frac{\int \left[\overline{g}^w(\mathbf{R})\right]^2 d^2R}{\sum_n w_n^2} \tag{8.3}$$

where $\overline{g}^w(\mathbf{R})$ is defined in Section 3.2.2. (As Appendix F shows, the right-hand side of Eqn 8.3 may be written in several alternative forms.) Equation (8.3) will be called the *integral relationship* or the *'energy conservation' relationship*. In the case of an array that is not shaded in any way ($w_n \equiv 1$, $\overline{g}(\mathbf{R})$ given by Eqn 3.19), this relation reduces to

$$\frac{J_i}{J_a} = \frac{c}{2}\left(\frac{\overline{\sigma}}{\sigma_{\text{rms}}}\right)^2 \frac{N\lambda_c^2}{S_{\text{ap}}} \tag{8.4}$$

The remaining subsections are arranged as follows. Sections 8.2, 8.3 and 8.4 are like an executive summary; while the detailed calculations are given in Sections 8.5 to 8.7 and the associated appendices. Section 8.2 gives the physical ideas behind the proposed relationship, in particular the parallel with true energy conservation for wave propagation. Section 8.3 discusses problems faced in making the extension from normal energy conservation to the

desired 'energy conservation' relationship. Section 8.4 summarises progress in establishing the desired relationship and gives the present status of that work.

Section 8.5 shows that, when the model of Section 2.2 is extended in the three ways discussed in Section 5, the integral relation continues to hold for a point target. Section 8.6 extends this result to a small, smooth ball. Section 8.7 relates the integral relation to a rough surface, but no proof is offered in that case.

8.2 The Parallel between the Integral Relationship and Energy Conservation

We now explain the ideas behind the proposed relationship between J_a (a sum-and-integral of the squared voltages) and J_i (an integral of the squared image amplitudes). Consider first J_a, and for a start consider the unweighted case $w_n \equiv 1$. Then J_a is proportional to the electrical energy produced in the receiving array by the pulse[33] (the subscript a is for 'array'). From (2.7), we may also say that J_a is proportional to *the energy input into the image reconstruction process.* In the weighted case, it is not immediately clear whether, in seeking a relationship between J_a and J_i, we should seek one that has E_n weighted by the factor w_n^2 (as in Eqn 8.1) or simply w_n. We have chosen w_n^2, because Equation (2.7) seems to imply unambiguously that the weighting process is equivalent to replacing every voltage $E_n(t)$ with $w_n E_n(t)$.

In regard to J_i, let us define a 'corrected' image intensity $\left|\overline{A}(\mathbf{r})\right|^2 r^{-2}\cos\theta$. The correction factor $r^{-2}\cos\theta$ may be argued for on simple geometrical grounds.[34] In the final analysis, that correction factor is needed so as to make the integral (8.2) for a point target independent of the position at which the target is placed. Then J_i is the volume integral of the corrected intensity. J_i may be thought of as *the total 'energy' in the image* (the subscript i is for 'image').

The proposed relationship parallels to some extent results in wave theory (in particular, acoustic or electromagnetic waves). For simplicity we consider the monofrequency case. Suppose there are several interfering waves. The intensity (acoustic or electromagnetic) at a

---

[33] Strictly, J_a is proportional to the energy that would be produced if the voltage from every element were fed into a resistance of 1 ohm. Since only the voltage, not the current, is used in image-forming, the actual value of the resistance does not matter.

[34] Given that the image-forming process (2.7) contains no spherical spreading factor, the factor r^{-2} seems eminently reasonable as a correction factor. The factor $\cos\theta$ comes from the last line of (B.2); it could be regarded either as a correction to the intensity or as a correction to the volume element. In the case of a point target, the factor $\cos\theta$ is associated with the stretching factor $1/\cos\theta_0$ that is applied to the PSF, discussed in Section 4.4.

given point is increased or decreased according to whether constructive or destructive interference has occurred. Nevertheless, in the context of an integration of the intensity over an effectively infinite surface, *the constructive and destructive effects cancel.* That is, the integral, say K, of intensity is the same as would be calculated from the sum of the integrals due to the various constituent waves treated individually. This is the first result. Second, if each individual wave can be attributed to a separate source, *the said integral, K, equals the sum of the powers from the sources.* These two results must hold, from energy conservation.

In the parallel, J_a is effectively the total 'energy' injected into the image; while J_i, the total 'energy' in the image, would be proportional to it. Different relative phasings of the voltage streams $E_n(t)$ at the various elements would lead to different patterns of constructive interference in the image, but would not affect the image's total 'energy' J_i.

The same basic idea was used by Tsao [1986] (described in Steinberg and Subbaram [1991, p. 259]) in proposing an 'energy conservation principle.' His principle was put to a quite different use, namely the choice of optimum array weights in a radar system. His 'basic idea' was reported by Steinberg and Subbaram as follows: 'Using Parceval's theorem, he [Tsao] argued that *the total image energy, being equal to the total signal energy in the aperture,* was independent of the distortion [due for example to a turbulent medium] and therefore independent of the distribution of the image energy in the image plane' (italics added).

8.3 Problems in Extending to the Desired 'Energy Conservation' Relationship

There appear to be three problems facing an attempt to 'extend' the result for waves to the desired result for image-forming (in the case of a *general* target). These three problems, to which a fourth will be added below, are as follows.

Problem 1. No wave propagates physically from the source; instead, an image is formed in software according to (2.7). However, let us for the moment put aside the problem that the image-forming is based on *two-way* propagation—recognised below as Problem 2. Then we have a passive system (one-way propagation). Then it can be shown (Appendix G) that the image-forming equation is, in a sense, equivalent to physical backpropagation—the time reverse of normal propagation. True energy conservation applies to the latter. This suggests that the real difficulties lie only with Problems 2 onward.

Problem 2. The source of 'backpropagated waves' is not the receiving array, but some combination of the transmitter with the receiving array. This is seen from the delays applied to E_n in Equation (2.7). This 'combining' adds considerable complexity.

Problem 3. Unlike the continuous-wave cases envisaged in Section 8.2, the 'backpropagated wave' generated by each stream $E_n(t)$ is a pulse or a superposition of pulses. Associated with this difference is a further difference: from (8.2), the proposed result is concerned with an integral, not over a surface, but over the entire volume.

These three problems are obstacles in the way of a proof of the integral relationship (8.3); but they do not rule out such a relationship.

$\overline{A}(\mathbf{r})$ was defined earlier (Section 3.2.2) as the image that would have been obtained if a *smoothed* element density $\overline{g}(\mathbf{R})$ had been used. If one attempts to estimate $\overline{A}(\mathbf{r})$ from $A(\mathbf{r})$ by *simple* means, apparently the only means available is to use the fact that $\overline{A}(\mathbf{r})$ is the result of taking the true image amplitude $A(\mathbf{r})$ and ignoring the contributions of the distant sidelobes (a recipe that admittedly does not fully pin down $\overline{A}(\mathbf{r})$). That recipe is adequate for a *point target*, as discussed in Section 3.2.2; it is also adequate for a collection of a few well-separated point targets. However for closely spaced point targets, or for an extended body, a problem arises—a problem different in kind to the three listed above. (In what follows we use the term 'clutter' to mean the contribution of the distant sidelobes.)

Problem 4. For non-simple targets, such as a collection of point scatterers whose PSFs overlap, it is not immediately clear what the clutter is. This is basically because, at the one location $\mathbf{r}$, there can coexist the main lobe from one target and clutter from another target. Thus it is not clear how to calculate the integral J_i (Eqn 8.2).

This fourth problem—at least if it is valid to model every scene by a collection of point scatterers—does not so much threaten to invalidate the relation (8.3) as to limit its application. To apply the integral relation to a system (as in Section 9) requires that one be able to estimate the clutter and then subtract it off.

Actually such estimation may be possible. First, for a relatively simple system, such as the arrangement of two rectangular targets discussed in Section 9, it may be possible to estimate the clutter without a complex calculation. Second, for a complex system, presumably one could proceed by treating the image as a collection of PSFs. Then one could subtract off the clutter by applying the CLEAN algorithm used in radio astronomy [Hogbom 1974; Clark 1980] and used more recently in radar imaging [Steinberg and Subbaram 1991].

8.4 Status of the General Proof of the Integral Relationship

As was seen in Section 8.3, the proof of the 'energy conservation' relation faces problems. Work (not presented here) is under way to deal with these. First, the relation is being tried out in test cases. A test case of particular interest involves reflection from an acoustic plane mirror—actually, a 1-D mirror in a 2-D acoustic system. This test case has considerable significance, as it is quite different from a point scatterer: it involves not only reflection from many points but the presence of coherence between these reflections. It is found that the relationship passes the test: J_i/J_a has the same value as for a single point scatterer in a 2-D system. Second, a general argument is being sought to establish the integral relationship. Some progress has been made in this area.

Note that the work of Tsao referred to in Section 8.2 makes it very likely that the basic idea of 'energy conservation' is correct.

A further point needs to be made. The immediate aim of this work on developing an 'energy conservation' relation is to analyse the results of the reflectivity experiment. The relevant steps in the analysis are: (i) to compare the reflections from two rectangular surfaces

('plates') to obtain ratios of reflection coefficients, and (ii) to calibrate, using a smooth ball target, to obtain absolute reflection coefficients. Consider step (i). Various ratios have been proposed as the key to the reflectivity ratio. These proposals involve, first, the question of how one should perform spatial averaging in order to improve the statistics. In particular, there is the question of whether, over the volume around the plate surface, one should combine (by addition) the image amplitudes $A(\mathbf{r})$ themselves or their squares. Second, the proposals involve whether, to obtain a quantity proportional to the reflection coefficient, one (i) simply looks for the maximum of $A(\mathbf{r})$ as a function of n, the coordinate normal to the plate surface, or (ii) takes an integral over n, as the integral relation given by (8.2) and (8.3) implies. Third, the proposals involve whether, when comparing two plates inclined at different angles, some correction factor such as $\cos i$ or $\cos R$ (Section 7) needs to be inserted. In opting for a particular answer to these questions, *it is far better to choose an option that has some theoretical backing than to select an answer on no basis at all.* Therefore at this stage there are pragmatic grounds for basing the analysis on the 'energy conservation' relation. How the integral relation answers these questions will be seen in Section 9.

8.5 Integral Relationship for the Extended Model

In Section 5, we introduced three extensions to the restricted basic model of Section 2.2—extensions needed so as to cover the arrangement of the reflectivity experiment. It was shown in Section 8.1 (Appendix F) that the integral relationship holds for a point scatterer in the original, unextended model. We now show that if the model is extended in any of the three ways—separately or together—the integral relationship continues to hold for a point scatterer. The proof is given in Appendix H.

8.6 Integral Relation for a Small, Smooth Ball

From Section 6.3, a smooth ball is equivalent to a *point target* located at (6.14) and having target strength (6.17), provided the ball is small enough to satisfy (6.15). Hence the integral relationship (8.3), including all the extensions discussed in Section 8.5, hold for the ball target as well.

8.7 Integral Relation for a Rough Surface

The rough surface was treated in Section 7. For such a surface the integral relationship (8.3) will not be proved. That relationship will however be *assumed* in Section 9 as a basis for analysing the data of the reflectivity experiment. The primary purpose of the present Section 8.7 is to evaluate J_a, one of the two factors that occur in the integral relationship. The value of J_i then follows automatically once the integral relationship is accepted.

The calculation of J_a is performed in Appendix I, where it is found that

$$J_a = (D_r \sigma_{\rm rms} H)^2 T_e \pi^{-1} S \rho \cos i \cos R \sum_n w_n^2 \tag{8.5}$$

Appendix I also gives the conditions needed for this result to hold. The appendix also shows that, in certain more general circumstances, the measurement described in Section 9 yields a certain *average* reflection coefficient.

9. Application to 'Reflectivity' Experiment

We now show how the integral relation, argued for in Section 8, may be used in the analysis of the DSTO/TUS/University of Sydney reflectivity experiment.[35]

9.1 Comparison of Plates

As discussed in Section 8.4, it is preferable to base the estimation of reflection coefficients on the integral relation, which has some theoretical basis, than on an assumption with no basis. An example of an assumption of the latter kind is that the peak of the image intensity over n (where n is the coordinate perpendicular to the plate) is proportional to the reflection coefficient, with a constant of proportionality that is independent of the angle of incidence. Essentially, that example assumes that the peak intensity, as opposed to some spatial integral of it, is a measure of the reflection coefficient.

The integral relationship proposed in Section 8 is applied as follows. When two of the planar targets are compared in a single image (see Fig. 6), from (8.3) and (8.5) we have[36]

$$\frac{(J_i)_p}{(J_i)_s} = \frac{(J_a)_p}{(J_a)_s} = \frac{\left[T_e (D_r \sigma_{\rm rms} H)^2 S \rho \cos i \cos R \sum_n w_n^2\right]_p}{\left[T_e (D_r \sigma_{\rm rms} H)^2 S \rho \cos i \cos R \sum_n w_n^2\right]_s} \tag{9.1}$$

Here p and s are the two targets, while the subscript p, for example, means 'evaluated for target p.' s means the 'standard' target, while p represents the variable target, which will be

[35] Certain complications occurring in the experimental results—speckle, clutter and instrumental noise—are not discussed here.

[36] Since $\overline{A}(\mathbf{r})$, not $A(\mathbf{r})$, appears in J_i in (9.1) and (8.2), it is assumed that the analysis involves a preliminary stage in which the clutter is estimated and then subtracted off.

called the 'object' target. Recall that ρ is the reflection coefficient *at the combination of angles* (i, R, g) concerned.[37]

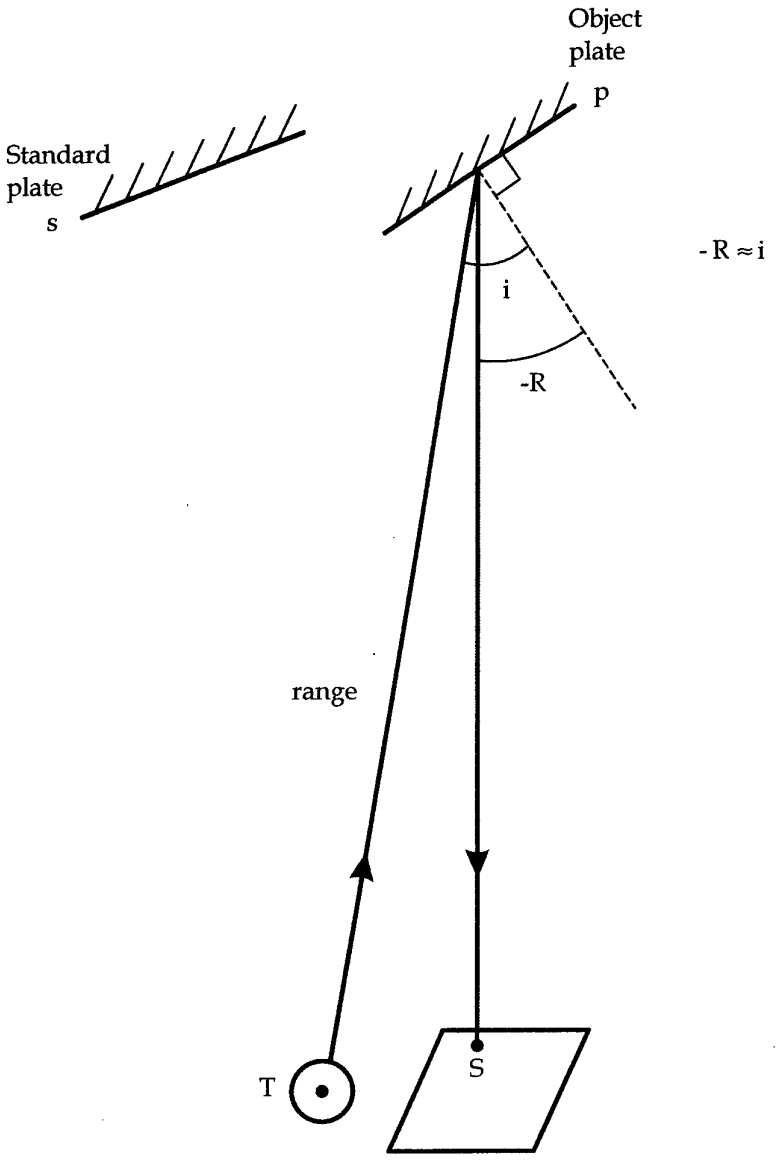

Figure 6: *Comparison of plates in the reflectivity experiment. T=transmitter, S=typical receiver element, i=angle of incidence, R=angle of reflection. We have* $-R \approx i$, *because* $TS \sim L << range$. *(We write minus R, because* $+R = i$ *would correspond to a specular reflection.)*

[37] For maximum accuracy the angles are determined by the ray travelling to the centre of the plate and thence to the centre of the array.

Consider the first equality of (9.1): it requires a supporting argument because, in the first instance, Section 8 says only that the equality applies when each of p and s is a *complete scene*. We wish to apply the equality when p and s are two targets forming *part of one total scene*. Consider first an uncorrelated (i.e. non-chirp) signal. Suppose that the return signals from p and s arrive at the receiving array in two time intervals that do not overlap. (This means essentially that the two targets do not overlap in range, and moreover are separated by at least a few range resolution lengths.) Then the value of J_a (integrated only over the times relevant to p) is the same as if p were the only target present.[38]

We now turn to J_i. Under the above circumstances, it should also be true that the image of each target is unaffected by the presence of the other target. Thus the value of J_i for p, for example, integrated over just the region of p (plus near sidelobes) should be the same as if p were the only target present. Then the first equality in (9.1) holds for the two co-present targets. The last expression in (9.1) is obtained immediately from (8.5).

Second, consider a correlated signal. At first sight this case is problematic because, in the experiment, the chirp length cT far exceeds the size (in range) of the plates. But because the whole system for propagation is linear, we are assured that the experimental results are the same as if a signal $Y(t)$ had been transmitted. Thus, consider the case, as in the experiment, where the *dechirped* return signals from p and s arrive at the receiving array in two non-overlapping time intervals (same as in the argument above regarding J_a and J_i, but now with the qualification 'dechirped'). Then the whole argument goes through as before, and (9.1) is shown to hold.

For many of the factors in the last expression of (9.1), the corresponding factors in the numerator and the denominator are equal and cancel, because both refer to the same image—for example T_e and $\sum_n w_n^2$. For a number of other factors, it is not too bad an approximation to again equate the respective quantities, though we can improve on that approximation if required. Applying equality to such pairs as seems reasonable, we obtain

$$\frac{(J_i)_p}{(J_i)_s} = \frac{[S\rho \cos i \cos R]_p}{[S\rho \cos i \cos R]_s} \tag{9.2}$$

Here the targets have been taken to be sufficiently near broadside so that the two values of D_r may be taken as equal; this is well justified in the experiment.

We now turn to the left-hand side of (9.2), given by (8.2). If the plate is large enough, the image intensity (at least if smoothed) should be constant over the plate.[39] Consequently (and treating θ and r as constants), from (8.2) we have, on the left-hand side of (9.2),

---

[38] Of course it is required also that there is negligible scattering from one target to the other and no 'shadowing.'

[39] The deviations from constancy should be of three types. First, there are diffraction effects at the edges. These should become relatively small when the plate becomes large. (In any case, probably a better approach to dealing with edge effects is to apply 'energy conservation' to a portion of the plate

$$(J_i)_p = \left[Sr^{-2} \cos\theta \int |A(\mathbf{r})|^2 \, dn \right]_p$$

where n is the coordinate normal to the plate. The analogous result holds for $(J_i)_s$.

These results are then substituted in (9.2). Then, letting, for example, r_p be the range of target p, when we put $r_p \approx r_s$, $\cos\theta_p \approx \cos\theta_s$, and also[40] (as in the experiment) $R_p \approx -i_p$, $R_s \approx -i_s$, Equation (9.2) becomes

$$\frac{\left[\int |A(\mathbf{r})|^2 \, dn \right]_p}{\left[\int |A(\mathbf{r})|^2 \, dn \right]_s} = \frac{\rho_p \cos^2 i_p}{\rho_s \cos^2 i_s} \tag{9.3}$$

Hence, from the experimental data, the ratio of the reflection coefficients can be determined. Then if the *absolute* reflection coefficient ρ_s of the standard plate is known, the coefficient ρ_p of the object plate is immediately determined. The calibration of the standard plate required for this step is discussed in the next Section 9.2.

Note that in practice, to reduce the effects of noise to a minimum (as discussed in Section 1.1), each of the two line integrals in (9.3) would be replaced by a volume integral. This replacement would be achieved by performing an extra surface integration, by summing (parallel to the plate's surface) over voxels, but ending the integration before reaching voxels close to the edge of the plate.

9.2 Calibration

For the ball (label b), we have the following comparison with the standard plate (label s). From (8.5), (F.1), (6.18) and Section 8.6, we obtain

$$\frac{(J_i)_s}{(J_i)_b} = \frac{(J_a)_s}{(J_a)_b} = \frac{\left[(D_r H)^2 \pi^{-1} S \rho \cos i \cos R \right]_s}{\left[(D_r H \, a/2)^2 \rho \right]_b} \tag{9.4}$$

---

that does not approach the edges.) Second, in the coherent case, constructive interference and destructive interference occur in different parts of the plate reflector, giving rise to speckle. Third, in the incoherent case, spatial fluctuations in the reflected intensity also occur due to the changing geometry, that is, due to the fact that the pattern of peaks and valleys varies from one part of the surface to another. (Perhaps this phenomenon is on a continuum with speckle.) In regard to the second and third phenomena, as the plate becomes large the image intensity becomes uniform in a coarse-grained sense.

[40] The experimental condition is not the condition for specular reflection. Rather, the pair of minus signs means that the experiment is approximately monostatic.

Here ρ_b, the reflection coefficient of the ball, is normally put equal to unity for a calibration; we now take this step. Then, when the same approximations are made as with the comparison of two plates, the equation becomes

$$\frac{(J_i)_s}{(J_i)_b} = \frac{[S\rho \cos^2 i]_s}{\pi(a/2)^2} \tag{9.5}$$

On the left-hand side, putting $r_s \approx r_b$, $\cos\theta_s \approx \cos\theta_b$ and, as in Section 9.1, approximating $\left[\int |A(\mathbf{r})|^2 dV\right]_s$ by S times a 1-D integral, we obtain

$$\frac{\left[\int |A(\mathbf{r})|^2 dn\right]_s}{\left[\int |A(\mathbf{r})|^2 dV\right]_b} = \frac{\rho_s \cos^2 i_s}{\pi(a/2)^2} \tag{9.6}$$

By using (9.6) and then (9.3), the absolute reflection coefficients are obtained, first for the standard target and then for all the object targets. (This statement is subject to the possible limitation mentioned in Section 7.1 concerning the smoother targets that may lead to coherent reflection).

10. Conclusion

The present work has been motivated by an experiment to measure the acoustic reflection coefficient of surfaces as a function of roughness and angle of incidence, with emphasis on the diffuse or nonspecular component. Consideration of how to analyse this experiment has led to the proposing of an integral relationship or 'energy conservation' relationship. In order to make this relationship plausible, it has been necessary to derive a number of results. These comprise the formulae for the 3-D image due to a point target, a small, smooth ball and a flat surface that reflects incoherently.

In regard to the point target, formulae for the image (point spread function) have been obtained under fairly general conditions. These include near field conditions. To increase generality, allowance has been made for a transmitter displaced in an arbitrary direction from the centre of the array, a spherical rather than a point transmitter, and a correlated (chirp) signal.

In regard to both the point target and the other targets, the conditions of validity for the formulae for the image have been carefully stated. If the conditions (mostly of the form $f << g$) are well met, the predictions hold with high accuracy. More common is the case where at least one of the conditions $f << g$ holds only to a borderline degree. In such cases

some predictions hold with only moderate accuracy. A common example concerns results that hold out to several sidelobes from the centre when the conditions are well met: when the conditions hold less well, these results often become semiquantitative outside the main lobe.

The integral relationship proposed is similar to the energy conservation relation in diffraction theory. The reasons have been given why that true energy conservation principle cannot be straightforwardly extended to obtain the desired relationship. Arguments have been presented which, though they do not amount to a proof, show the plausibility of the proposed integral relationship. Work is in hand which attempts to find a general proof.

Finally it has been shown how the integral relationship would be applied in the analysis of the experiment to produce the reflection coefficients.

11. Acknowledgements

The author thanks Ian S. F. Jones for his encouragement of the present work. In the reflectivity experiment relating to the present work (actually Phase 1 of a longer experiment), the experimental design and experimental work were carried out by the Maritime Operations Division (MOD) of DSTO together with Thales Underwater Systems (TUS). TUS provided the experimental acoustic imaging device and constructed the jig to position the targets. The Ocean Technology Group of the University of Sydney carried out the detailed analysis done so far. Darryl McMahon is thanked for his useful comments on the report.

12. References

Blair, D.G. and Anstee, S.D. (2000). *Underwater Acoustic Imaging: A Simulation Program and Related Theory* (AMRL Technical Note DSTO-TN-0274). Melbourne: Aeronautical and Maritime Research Laboratory.

Blair, D.G., Bedwell, I., Anstee, S.D. and Li, Y. (1994). Use of a Random Array for High-Resolution Underwater Acoustic Imaging. *Internat. Conf. On Underwater Acoustics,* University of New South Wales, 5–7 Dec. 1994, pp. 56–57. Darlinghurst, N.S.W.: Australian Acoustical Soc.

Blair, D.G. and Jones, I.S.F. (1998). *Underwater Acoustic Imaging: Rapid Signal Processing* (DSTO Technical Note DSTO-TN-0098). Melbourne: Aeronautical and Maritime Research Laboratory.

Clay, C.S. and Medwin, H. (1977). *Acoustical Oceanography: Principles and Applications.* New York: John Wiley.

Clark, B.G. (1980). An Efficient Implementation of the Algorithm CLEAN. *Astron. Astrophys.*, **89**, pp. 377–378.

Ditchburn, R.W. (1952). *Light.* London: Blackie.

Gradshteyn, I.S. and Ryzhik, I.M. (1965). *Tables of Integrals, Series and Products.* New York: Academic Press.

Grandy, W.T. (2000). *Scattering of Waves from Large Spheres.* Cambridge, UK: Cambridge University Press.

Hogbom, J. (1974). Aperture Synthesis with a Non-Regular Distribution of Interferometer Baselines. *Astrophysics Journal Supplement,* **15**, pp. 417–426.

Jerlov, N.G. (1976). *Marine Optics.* Amsterdam: Elsevier.

Jones, I.S.F. (1996). *Underwater Acoustic Imaging Innovation Program* (DSTO Technical Note DSTO-TN-0065). Melbourne: Aeronautical and Maritime Research Laboratory.

Longhurst, R.S. (1957). *Geometrical and Physical Optics* (Student's Edition). London: Longmans.

Madry, A. (2000). *Acoustic Reflectivity at Megahertz Frequencies.* Ocean Technology Group, Report 8/00. Sydney: University of Sydney.

Maguer, A., Vesetas, R. and Azemard, F. (2000). 3D Acoustic Imaging of Objects in Water. *Acoustics 2000: Proceedings of Australian Acoustical Society Annual Conference,* held at Joondalup Resort, Western Australia, 15–17 Nov. 2000, pp. 87–93. Perth, W.A.: Australian Acoustical Society.

Maynard, J.D., Williams, E.G. and Lee, Y. (1985). Nearfield Acoustic Holography (NAH): 1. Theory of Generalized Holography and the Development of NAH. *Journal of the Acoustical Society of America,* **78**, pp. 1395–1413.

Meyer, E. and Neumann, E.-G. (1972) (trans. By J.M. Taylor). *Physical and Applied Acoustics – An Introduction.* New York: Academic Press.

Morse, P.M. and Ingard, K.U. (1968). *Theoretical Acoustics.* New York: McGraw-Hill.

Murino, V. and Trucco, A. (2000). Three-Dimensional Image Generation and Processing in Underwater Acoustic Vision. *Proceedings of the IEEE,* **88**, pp. 1903–1946.

Perez-Matzumoto, A.E., Fahy, F.J. and Elliot, S.J. (1989). *Near-Field Acoustic Holography* (ISVR Technical Report No. 179). Southampton, England: Institute of Sound and Vibration Research, University of Southampton.

Smith, S.W., Pavy, H.G. and von Ramm, O.T. (1991). High-Speed Ultrasound Volumetric Imaging System—Part I: Transducer Design and Beam Steering. *IEEE Transactions on Ultrasonics, Ferroelectrics and Frequency Control,* **38**, pp. 100–108.

Steinberg, B.D. (1976). *Principles of Aperture and Array System Design – Including Random and Adaptive Arrays.* New York: John Wiley.

Steinberg, B.D. and Subbaram, H.M. (1991). *Microwave Imaging Techniques.* New York: John Wiley.

Sutton, J.L. (1979). Underwater Acoustic Imaging. *Proceedings of the IEEE*, **67**, pp. 554–566.

Tsao, J. (1986). Phased Array Beamforming by the Parceval's Theorem. *IEEE AP-S Symposium Digest*, IEEE AP-S Internat. Symposium, Philadelphia, PA, June 1986, Vol. 1, pp. 335–338.

Urick, R.J. (1983). *Principles of Underwater Sound*, 3rd Ed. New York: McGraw-Hill.

Williams, J. (1970). *Optical Properties of the Sea.* Annapolis, Maryland: United States Naval Institute.

Appendix A: Shaded Arrays

As mentioned in Section 3.2.3, three cases are to be discussed, each involving a different kind of element shading. The cases are as follows. Case (i): The density of elements varies (but not too rapidly) over the aperture. Case (ii): Shading (weighting) is applied to the array during the image-forming, usually in software. Case (iii): The element strength (sensitivity) is itself shaded over the aperture.

In case (i), the theory is already covered by Sections 3.2.1 and 3.2.2 with the introduction of $\bar{g}(\mathbf{R})$ above (3.18); $w(\mathbf{R})$ is put equal to unity.

The obtaining of $\bar{g}(\mathbf{R})$ from $g(\mathbf{R})$ by smoothing can be discussed in more detail, as follows. The smoothing is performed over a distance much greater than the separation of the elements, but much less than the size of the aperture. One procedure we may adopt —the crudest procedure—is to subdivide the aperture into distinct 'smoothing regions.' For each $\mathbf{R}$, one then takes a mean over the smoothing region containing $\mathbf{R}$. Thus

$$\bar{g}(\mathbf{R}) = \left(S^1\right)^{-1} \int^1 g(\mathbf{R}) d^2R = N^1/S^1$$

Here the superscript 1 refers to the smoothing region; S^1 is its area and N^1 the number of elements in the region. Thus, as expected, $\bar{g}(\mathbf{R})$ comes out to be an estimate—somewhat crude—of the local element density. An alternative procedure for obtaining $\bar{g}(\mathbf{R})$ from $g(\mathbf{R})$ is to remove the higher spatial frequency components from $g(\mathbf{R})$.

Case (ii) is dealt with by the factor w_n or $w(\mathbf{R})$in (2.7). It remains to remark that because the multiplicative combination $w(\mathbf{R})\bar{g}(\mathbf{R})$ appears (implicitly) in (3.18), then the following holds. Suppose that initially there is an unweighted array ($w(\mathbf{R}) = \text{const.}$) with a uniform distribution of elements ($\bar{g}(\mathbf{R}) = \text{const.}$). Then the effect of introducing a given weighting $w(\mathbf{R}) = w_0(\mathbf{R})$ is the same as the effect of introducing an identical shading in the number density, i.e. the effect of putting $\bar{g}(\mathbf{R}) \propto w_0(\mathbf{R})$.

Case (iii) requires a modification of the model of Section 2. The shading factor in the physical element strength, say s_n or $s(\mathbf{r}_n)$, is to be superposed multiplicatively on the distribution of σ discussed below Equation (2.16). Thus the physical element strength is $s_n\sigma_n$, where s_n varies smoothly with position and σ_n still has the properties given below Equation (2.16). Thus s_n should be inserted on the right-hand side of (2.4), but Equation (2.7) remains as written. As far as the calculation of $\bar{A}_0(\mathbf{r})$ is concerned, the introduction of the strength shading s_n is equivalent to the application of a weight $w_n \propto s_n$ during image-forming (in the case where the array initially has $w_n = \text{const.}$). Therefore the theory of Sections 3.2.1 and 3.2.2 (in particular, Eqn 3.18 with $s(\mathbf{R})$ replacing $w(\mathbf{R})$) covers this case also.

Appendix B: Integral of the Squared Directivity

Here remarks are made in respect of two aspects of the integral (3.30). First, note that in Equation (3.30), the 'element' $du\,dv$ is *not* equal to the element of solid angle, which is

$$d\Omega = \sin\theta\, d\theta\, d\phi \tag{B.1}$$

The relation between $du\,dv$ and $d\theta\,d\phi$ is given by the Jacobian J as follows:

$$\begin{aligned} du\,dv = J\,d\theta\,d\phi &= \begin{vmatrix} \partial u/\partial\theta & \partial u/\partial\phi \\ \partial v/\partial\theta & \partial v/\partial\phi \end{vmatrix} d\theta\,d\phi \\ &= \sin\theta\cos\theta\, d\theta\, d\phi \\ du\,dv &= \cos\theta\, d\Omega \end{aligned} \tag{B.2}$$

where (3.14) and (B.1) have been used.

Second, Equation (3.31), giving the value of the integral, may be written in another way by introducing a *shading correction factor* Q:

$$Q = \frac{\left[\int\left[\bar{g}^{w}(\mathbf{R})\right]^2 d^2R\right]\left[\int d^2R\right]}{\left[\int \bar{g}^{w}(\mathbf{R})\, d^2R\right]^2} \geq 1 \tag{B.3}$$

where all integrals are over the aperture. Q is independent of the magnitude of both S_{ap} and N, and depends only on the shape of the distribution $\bar{g}^{w}(\mathbf{R})$ (and the shape of the aperture). Then from (3.31) and the normalisation (2.8), we have

$$\int\left|D(u-u_0, v-v_0)\right|^2 du\,dv = \frac{\lambda_c^2}{S_{\text{ap}}} Q \tag{B.4}$$

where $Q = 1$ for an unshaded array (i.e. $\bar{g}^{w}(\mathbf{R}) = \text{const.}$). The general inequality $Q \geq 1$ in (B.3) follows immediately from the Cauchy-Schwarz inequality, which states that

$$\left|\int_R fg\, dx\right|^2 \leq \left[\int_R |f|^2\, dx\right]\left[\int_R |g|^2\, dx\right]$$

where the region R may have any number of dimensions but lies in a space of real variables only.

Appendix C: Detailed Calculation of a Point Spread Function

The case considered is specified by (i), (ii) and (iii) of Section 4.1. To treat this 3-D situation, we must go back to Equation (3.5) rather than Equation (3.8), since $r \neq r_0$ and so the rect factor must be retained. Using assumptions (i) and (ii) and using (3.9), we obtain from (3.5)

$$\overline{A}_0(\mathbf{r}) = D_r a_0 H \overline{\sigma} \int \exp\left[j \frac{2\pi}{\lambda} \zeta(\mathbf{R}) \right] \mathrm{rect}\left[\frac{1}{cT} \zeta(\mathbf{R}) \right] \overline{g}(\mathbf{R}) d^2\mathbf{R} \tag{C.1}$$

where

$$\zeta(\mathbf{R}) = 2(r - r_0) - (\hat{r} - \hat{r}_0) \cdot \mathbf{R} \tag{C.2}$$

In (C.1), from (3.19), $\overline{g}(\mathbf{R})$ is equal to $4N/\pi D^2$ for $\mathbf{R}$ in the circular region $X^2 + Y^2 < (D/2)^2$ and zero outside (see Fig. 5).

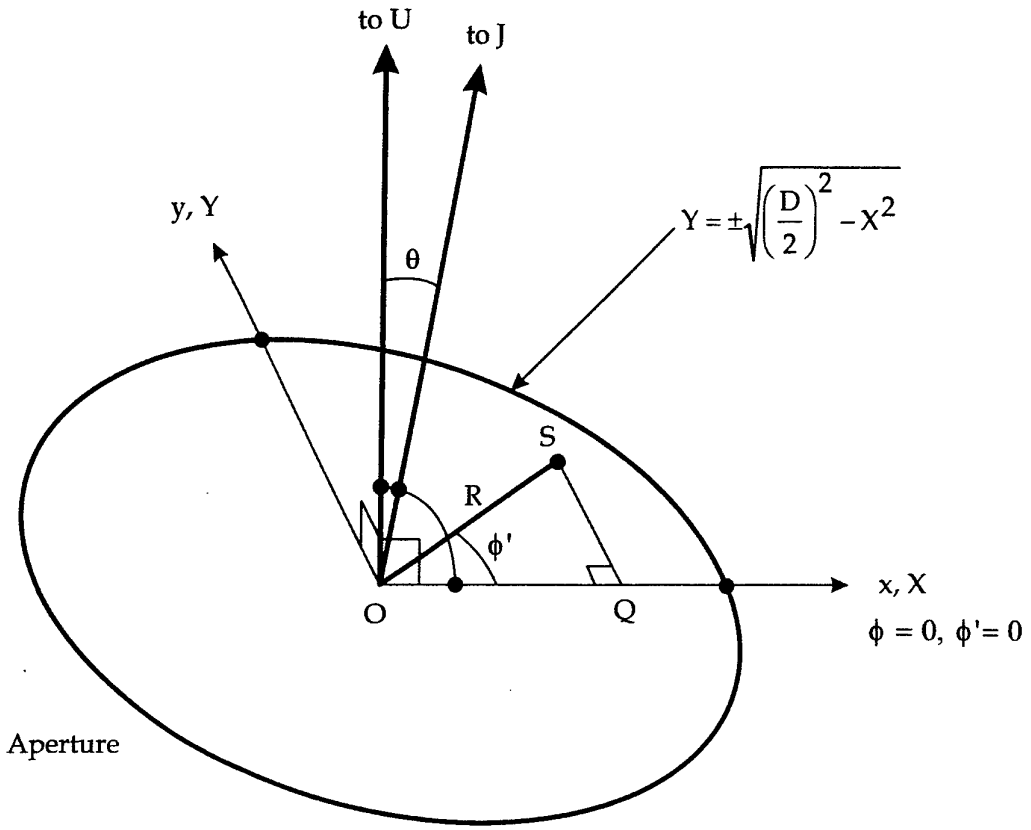

Figure 7: *Geometry for calculating beam pattern of a circular aperture. The point target (U) is at broadside. The image point J has coordinates* $(r,\theta,0)$ *or* $(x,0,z)$*. A typical receiving point S has coordinates* (R,ϕ') *or* (X,Y)*.*

We now invoke assumption (iii) to obtain

$$\overline{A}_0(\mathbf{r}) = D_r a_0 H \overline{\sigma} \frac{4N}{\pi D^2} \exp\left[j\frac{4\pi}{\lambda}(r - r_0)\right] \int_0^{2\pi} \int_0^{D/2} \exp\left[-j\frac{2\pi}{\lambda} R\sin\theta\cos\phi' \right] \mathrm{rect}[E_3]\, R\, dR\, d\phi' \tag{C.3}$$

with

$$E_3 = \frac{1}{cT}[2(r - r_0) - R\sin\theta\cos\phi']$$

Here the target at r_0 has a θ coordinate of 0, the image point is at (r, θ, ϕ), where we have put $\phi = 0$ due to the symmetry of the problem. The receiving point **R** has been represented in polar coordinates by (R, ϕ').

Now the two transition points for the rect function are given by

$$2(r - r_0) - R\sin\theta\cos\phi' = \pm\tfrac{1}{2}cT \tag{C.4}$$

Let us determine the condition under which the second term on the left-hand side is always small compared to the right-hand side; under that condition we shall be justified in dropping the second term. For a sufficient condition, we may put $R = D/2$ and drop the cosine; we thus have

$$D\sin\theta << cT \tag{C.5}$$

as the condition. With the second term dropped, it is convenient to rewrite the integral in (C.3) – call it I – in Cartesian coordinates; thus

$$I = \mathrm{rect}\left[\frac{2(r - r_0)}{cT}\right] \int_{-D/2}^{D/2} \int_{-\sqrt{(D/2)^2 - X^2}}^{\sqrt{(D/2)^2 - X^2}} \exp\left[-j\frac{2\pi}{\lambda} X\sin\theta \right] dY\, dX$$

where $\mathbf{R} = (X, Y)$ (see Fig. 5). Note that it has been possible to take the rect function in front of the integral sign. The Y integral is now trivial, and the X integral may be performed with the aid of the tabulated integral [Gradshteyn and Ryzhik 1965, p. 321]

$$\int_{-1}^{1} (1 - x^2)^{\nu - 1} e^{j\mu x}\, dx = \sqrt{\pi}\left(\frac{2}{\mu}\right)^{\nu - \frac{1}{2}} \Gamma(\nu) J_{\nu - \frac{1}{2}}(\mu)$$

which holds when the real part of ν exceeds zero. Here J is a Bessel function, Γ is the gamma function and $\Gamma(\frac{3}{2}) = \frac{1}{2}\sqrt{\pi}$. (Before performing the integration, inside the integral we

may replace j by $-j$ due to an antisymmetry with respect to X.) The result is Equation (4.1).

The conditions imposed in Sections 2 and 3 have been augmented by Equation (C.5). That particular condition can be simplified. This is because our formulae for the PSF are only required to hold in the first few lobes; hence $\sin\theta \lesssim \lambda/D$. Hence a sufficient condition is

$$D(\lambda/D) << cT, \quad \text{i.e.} \quad \lambda << cT$$

$$\text{i.e.} \qquad fT >> 1 \qquad \text{(C.6)}$$

But recall that we have already imposed the condition $fT >> 1$ at (3.17). Thus, without the imposition of any more conditions, the second term in (C.4) is negligible and our dropping of it is justified.

Appendix D: Derivation of Results for Transmitter Not in the Array Plane

In this appendix, we take the origin to be at the centre of the receiving array, i.e. we put $\mathbf{r}_c = 0$. Consider the (point) transmitter to be at a location $\mathbf{r}_t$ not necessarily in the array plane. For a point target, the voltage stream is obtained by an appropriate simplification of Equation (2.6) (p_{tra} replaced by (2.2), b replaced by zero in two places). As in Section 2.2, we now (i) make the approximation that $D_{rn} = D_r$ is independent of n, and (ii) impose the condition $r_0 >> L$ (as made in Eqn 2.14), so that the spherical spreading factor is simplified. We also impose essentially the conditions (2.15), associated with attenuation, in the form

$$\alpha L \sin\theta_0 << 1 \quad \text{and} \quad \alpha \left|(\mathbf{r}_t)_{xy}\right| \sin\theta_0 << 1 \tag{D.1}$$

Here the subscript xy refers to the component of $\mathbf{r}_t$ in the plane of the array (xy plane). Because $\mathbf{r}_t$ may now lie out of that plane, a further condition is required in order to ensure that H (now defined with the new attenuation factor containing the more general $\mathbf{r}_t$ in Eqn 2.6, but reducing to Eqn 2.13) is independent of both n and the transmitter location. That further condition is found to be

$$\alpha \left|(\mathbf{r}_t)_z\right| \cos\theta_0 << 1 \tag{D.2}$$

where the subscript z means perpendicular to the array plane. The spherical spreading factor simplifies because of Equation (2.9) and the condition $r_0 >> L$ mentioned above. Hence the voltage stream becomes (in place of 2.11)

$$E_n(t) = D_r a_0 H \sigma_n \xi\left[t - c^{-1}\left(\left|\mathbf{r}_0 - \mathbf{r}_t\right| + \left|\mathbf{r}_0 - \mathbf{r}_n\right|\right)\right] \tag{D.3}$$

Comparing (2.11), we see that we may also write

$$E_n^{\text{TAany}}(t) = E_n^{\text{TACA}}\left[t - c^{-1}\left(\left|\mathbf{r}_0 - \mathbf{r}_t\right| - r_0\right)\right] \tag{D.4}$$

When the convention $\mathbf{r}_c = 0$ for the origin is dropped, this equation becomes (5.1).

From (2.7), we also have (in place of 2.18)

$$A_0(\mathbf{r}) = D_r a_0 H \bar{\sigma} \sum_n w_n \xi\left[c^{-1}\left(|\mathbf{r}-\mathbf{r}_t| - |\mathbf{r}_0-\mathbf{r}_t| + |\mathbf{r}-\mathbf{r}_n| - |\mathbf{r}_0-\mathbf{r}_n|\right)\right] \tag{D.5}$$

We shall show that, subject to certain conditions,

$$\left[\overline{A}_0(\mathbf{r})\right]_{\text{TAany}} = \left[\overline{A}_0(\mathbf{r})\right]_{\text{TACA}} \times e^{j\phi} \tag{D.6}$$

where ϕ is real (i.e. Eqn 5.2). ϕ is equal to ϕ_2 in the relationship (D.10) below.

To show (D.6), we have, in (D.5), the expansion

$$|\mathbf{r}-\mathbf{r}_t| - |\mathbf{r}_0-\mathbf{r}_t| = (r-r_0) - (\hat{r}-\hat{r}_0)\cdot\mathbf{r}_t + \cdots; \tag{D.7}$$

this is the expansion to first order in $\mathbf{r}_t$, similar to an expansion in Section 3.1. Consequently, provided

$$|(\hat{r}-\hat{r}_0)\cdot\mathbf{r}_t| << cT_e \tag{D.8}$$

from the discussion at (4.4), we may write, with ϕ_1 and ϕ_2 real,

$$\begin{aligned}\xi(\text{as in D.5}) &= \xi_v(\text{as in D.5}) \times \exp(j\phi_1) \\ &= \xi_v(\text{as in 2.18}) \times \exp(j\phi_1) \\ &= \xi(\text{as in 2.18}) \times \exp(j\phi_2)\end{aligned} \tag{D.9}$$

where[41]

$$\phi_2 \approx -2\pi f_c c^{-1}(\hat{r}-\hat{r}_0)\cdot\mathbf{r}_t \tag{D.10}$$

Since ϕ_2 is independent of n, when the last line of (D.9) is substituted in (D.5), $\exp(j\phi_2)$ may be taken outside the summation. The result (D.6) follows with $\phi = \phi_2$.

The condition (D.8) may be written more simply. Since we are concerned only with the first few lobes, (D.8) becomes, as a *sufficient* condition,

$$(\lambda_c / L\cos\theta_0) r_t << cT_e \tag{D.11}$$

[41] Note that (D.10) holds in the sense that the ratio of the two sides is very close to unity (apart from unfavourable orientations of the vectors, when ϕ is small anyway). It has *not* been shown that the difference between the two sides is small compared to $\pi/2$.

(Here we have assumed that the most unfavourable alignment occurs in the case where both $\mathbf{r}_t$ and $\hat{r}-\hat{r}_0$ lie in the plane of the arc of increasing θ.) Because we have imposed the condition (2.9), the sufficient condition reduces to

$$f_c T_e \cos\theta_0 >> 1 \tag{D.12}$$

Thus, in order for (D.6) to hold, a slightly strengthened version of the condition (4.7) is required.[42]

Finally we discuss the magnitude of the phase shift ϕ introduced into $\overline{A}_0(\mathbf{r})$. From (D.10), ϕ is clearly zero when $\mathbf{r}$ is displaced from $\mathbf{r}_0$ along the range direction. It is of interest to estimate the phase change when the displacement is in the direction of increasing angle θ. Consider first the case where: (i) $\mathbf{r}_t$ is in the xy plane, (ii) the broadside direction and the two vectors, $\mathbf{r}_t$ and $\mathbf{r}_0$, lie in the same plane, and (iii) $r_t = \frac{1}{2}L$. Then, when $\mathbf{r}$ has moved to the first node of the beam pattern,

$$\begin{aligned}\phi &= \pm 2\pi \frac{1}{\lambda_c}\frac{\lambda_c}{L\cos\theta_0}\frac{L}{2}\cos\theta_0 \\ &= \pm\pi\end{aligned}$$

Second, consider the case where: (i) $\mathbf{r}_t$ is perpendicular to the xy plane, and (ii) $r_t = \frac{1}{2}L$. Then, at the first node, we get

$$\phi = \pm\pi\tan\theta_0$$

---

[42] Besides the conditions listed above in this appendix, there is a restriction required on the range difference, $r-r_0$. It arises from the requirement that the *second-order* term in (D.7) must also be small compared to cT_e. But this restriction turns out to be easily satisfied provided that the point $\mathbf{r}$ is in the first few range sidelobes.

Appendix E: Validity of Treating a Ball as a Point Scatterer

We find the condition under which a point target at the location (6.14) is an adequate representation of the ball. Let C be the centre of the array and let T be the location of the point transmitter. As in Section 5.1, T may be in or out of the array plane. Then A (6.14) lies on the line joining B, the centre of the ball, to M, the midpoint of TC (see Fig. 8). Let S be the location of a typical receiver element, and let D be the point at which reflection to S truly occurs. To a sufficient approximation, D lies on the line BN, where N is the midpoint of TS. (Note that not all of the above points are coplanar.) Now in (6.10), $E_n(t)$ is, in essence, sensitive only to the path length TDS. The point approximation replaces the path TDS with TAS. We require the difference between these to be small on a wavelength scale.

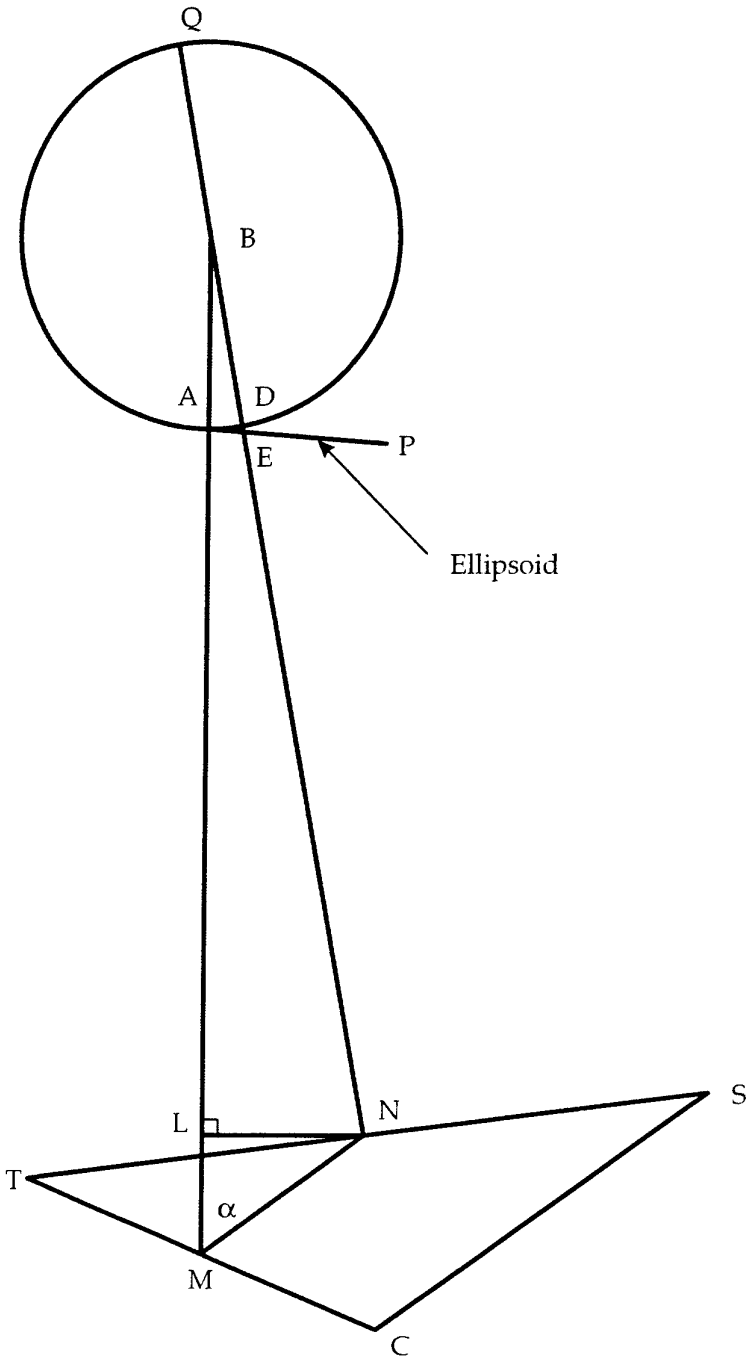

Figure 8: *Validity of treating ball as a point scatterer. T=transmitter, C=centre of array, S=typical receiver element. M and N are midpoints of TC, TS respectively. A and D are the points of intersection of the ball's surface with BM and BN respectively. To a sufficient approximation, reflection to S takes place at D; the point scatterer assumption takes this reflection to occur at A. B, A, M, N and D lie in a plane, but T, C and S normally do not lie in that plane. P is a typical point on the ellipsoid that has foci at T and C and passes through A; E is the point where the ellipsoid meets BN. See text.*

Now let P be a typical point on the ellipsoid (a surface of revolution) that has foci at T and C and passes through A. Then TP + PC is constant over the ellipsoid. Also, from Fermat's principle (stationary path principle) [Ditchburn 1952, p. 216], *this ellipsoid is tangential to the ball* at A. Let the ellipsoid intersect BDN at E. Then, within the approximations already made, the path difference is

$$\text{length TDS - length TAS} = 2(\text{DE}) \tag{E.1}$$

Now the radius of curvature of the ellipsoid at A is $\approx r_0$; this is much greater than the radius of the ball, *a*. Hence, in calculating DE, we may replace the ellipsoid with the tangent plane. From a theorem in geometry,

$$\text{AE}^2 = \text{DE.EQ}$$

where Q is the intersection of NB with the ball on the opposite side of the ball to D. Thus

$$\text{DE} \approx \text{AD}^2/\text{DQ} \tag{E.2}$$

But by similar triangles, since $a << r_0$,

$$\text{AD} = (\text{MN}\sin\alpha)(a/r_0) \leq \tfrac{1}{2}(\text{CS})(a/r_0) \tag{E.3}$$

where α is the angle NMB. A little thought shows that $\sin\alpha = 1$ is actually attained for some positions in the array (some orientations of CS) so that, for the worst position, '$\leq$' in (E.3) may be replaced by equality. At such orientations, consider extreme values of the element position S: at one extreme, $\text{CS} = \frac{1}{2}L$, so $\text{MN} = \frac{1}{4}L$. Combining this with Equations (E.2) and (E.3), we obtain

$$\text{DE} = \frac{1}{2a}\left(\frac{1}{4}\frac{a}{r_0}L\right)^2 = \tfrac{1}{32}a\left(\frac{L}{r_0}\right)^2 \tag{E.4}$$

For negligible error due to the altered path length, we require

$$2(\text{DE}) << \tfrac{1}{4}\lambda_c$$

This condition reduces to the final result (6.15).

Appendix F: Proof of the Integral Relationship for a Point Target

As stated before Equation (8.3), it will be shown that for a point target, the ratio J_i/J_a is a constant, independent of the position (r_0,θ_0,ϕ_0) of the target and also independent of its strength a_0. In the process we evaluate J_a, J_i and the ratio J_i/J_a, obtaining the result (8.3). The derivation in this appendix is confined to the unextended model of Section 2.2.

First we evaluate J_a for a point target by substituting (2.11) in (8.1), obtaining

$$J_a = (D_r a_0 H)^2 \int \sum_n \sigma_n^2 w_n^2 \left| \xi\left[t - c^{-1}\left(r_0 + |\mathbf{r}_0 - \mathbf{r}_n|\right)\right] \right|^2 dt$$

By a translation of the variable of integration, the argument of ξ may be replaced by simply t, and the integration is readily performed using (4.3). Then using (2.17), we obtain

$$J_a = (D_r \sigma_{\text{rms}}\, a_0 H)^2 T_e \sum_n w_n^2 \tag{F.1}$$

Note that the response (F.1) of the array *has no* $\cos\theta_0$ *factor.* This result may seem surprising. After all, each element presents to the rays returning from the target a projected area that is reduced (compared to broadside) by a factor $\cos\theta_0$. However the reason why (F.1) is independent of θ_0 is that each element responds simply to the pressure on it, the full pressure being felt at each point on the surface regardless of the angle of incidence. This having been said, *there is* in general a fall-off of response with angle! But this fall-off is due to the presence of the *directivity factor* D_r in (F.1).

We turn to the integral J_i. From (8.2) and (4.10), we obtain

$$J_i = (N D_r \bar{\sigma}\, a_0 H)^2 \int \left| \xi\left[\frac{2}{c}(r - r_0)\right] \right|^2 |D(u - u_0, v - v_0)|^2 \frac{\cos\theta}{r^2} d^3 r \tag{F.2}$$

But from (B.2), an expression in (F.2) becomes

$$\frac{\cos\theta}{r^2} d^3 r = \frac{\cos\theta}{r^2} dr\, r^2 d\Omega = dr\, du\, dv$$

The range or r integral is now performed using (4.3), so that (F.2) becomes

$$J_i = (N D_r \bar{\sigma}\, a_0 H)^2 (c/2) T_e \int |D(u - u_0, v - v_0)|^2 du\, dv$$

Now, in the argument of D, u_0 and v_0 may be dropped. This last integral is evaluated at (3.31) and (B.4), so that the final result for J_i is

$$J_i = N^2 (D_r \overline{\sigma} a_0 H)^2 \frac{c}{2} T_c \frac{\lambda_c^2}{S_{ap}} Q \tag{F.3}$$

where Q is given by (B.3).

From (F.1) and (F.3), the ratio J_i / J_a for a point target is

$$\frac{J_i}{J_a} = \frac{c}{2} \left(\frac{\overline{\sigma}}{\sigma_{rms}} \right)^2 \frac{\lambda_c^2 N^2}{S_{ap}} \frac{Q}{\sum_n w_n^2} \tag{F.4}$$

This expression may be written in several alternative forms. First, using (B.3) for Q and Equation (3.22), we obtain[43] the result, Equation (8.3), given in the main text. Further manipulation leads to

$$\frac{J_i}{J_a} = \frac{c}{2} \left(\frac{\overline{\sigma}}{\sigma_{rms}} \right)^2 \lambda_c^2 \frac{\int w(\mathbf{R}) \overline{g}^w(\mathbf{R}) \overline{g}(\mathbf{R}) d^2 R}{\int w(\mathbf{R}) \overline{g}^w(\mathbf{R}) d^2 R}$$

On the right-hand side, the last ratio is seen as a particular weighted average value of $\overline{g}(\mathbf{R})$, the latter being the smoothed element density. The ratio is therefore of order N/S_{ap}. Clearly if there is no shading of any kind ($w_n \equiv 1$, $\overline{g}(\mathbf{R})$ given by Eqn 3.19), the ratio equals N/S_{ap} and Equation (8.4) holds. Finally we may write

$$\frac{J_i}{J_a} = \frac{c}{2} \left(\frac{\overline{\sigma}}{\sigma_{rms}} \right)^2 \frac{\lambda_c^2 N}{S_{ap}} P \tag{F.5}$$

where P is of order unity and may be written as

$$P = \frac{\left\{ \int d^2 R \right\} \left\{ \int [w(\mathbf{R})]^2 [\overline{g}(\mathbf{R})]^2 d^2 R \right\}}{\left\{ \int \overline{g}(\mathbf{R}) d^2 R \right\} \left\{ \int [w(\mathbf{R})]^2 \overline{g}(\mathbf{R}) d^2 R \right\}}$$

[43] Here and in the sequel, it is necessary, in an integral, to replace $\overline{g}(R)$ by $g(R)$ or vice versa, in circumstances where this is an excellent approximation.

Appendix G: Backpropagation

Backpropagation has been reviewed by Maynard *et al.* [1985] and by Perez-Matzumoto *et al.* [1989]. The basic problem answered by backpropagation is as follows: Given the pressure field $p(\mathbf{r}',t)$ over a plane ($\mathbf{r}'$ = typical location on plane), reconstruct throughout a half-space the field $p(\mathbf{r},t)$ that gave rise to it (see Fig. 9). The required formula, in the monofrequency case, is given by Sutton [1979]:

$$p_f(\mathbf{r}) = \frac{jf}{c}\int \cos(\hat{n}, \mathbf{r}-\mathbf{r}')\frac{e^{jc^{-1}2\pi fR}}{R} p_f(\mathbf{r}')dS' \qquad \text{(G.1)}$$

Here p_f denotes the Fourier component of the pressure field (analytic signal) of frequency f, $\hat{n}$ is the outward unit normal to the receiving plane, $(\mathbf{A},\mathbf{B})$ denotes the angle between vectors **A** and **B**, $R = |\mathbf{r}-\mathbf{r}'|$ and the integral is over the $\mathbf{r}'$ plane. The result (G.1) is subject to the condition that all the distances R involved are large compared to a wavelength. This is a very weak condition, easily satisfied in underwater acoustic imaging applications.

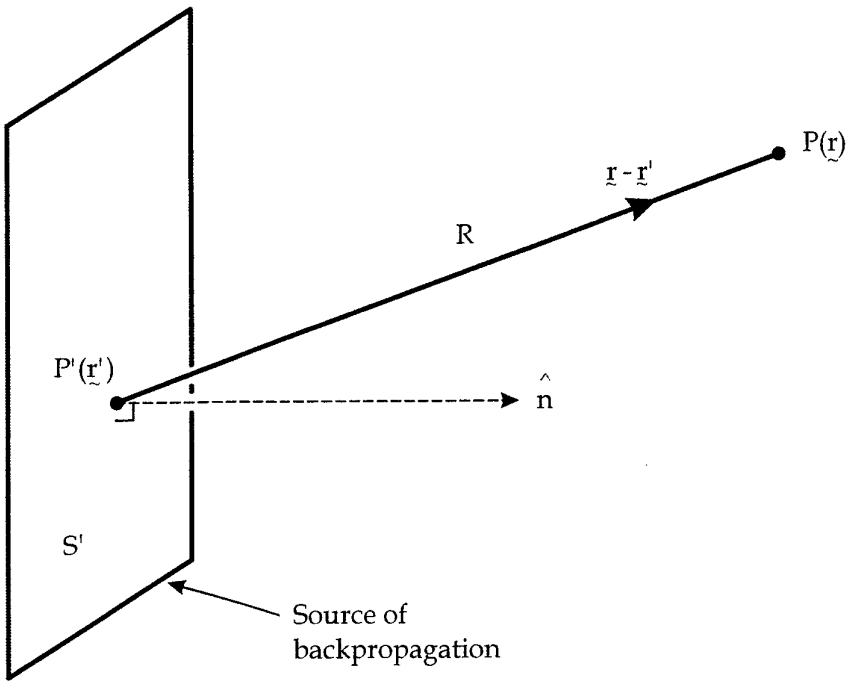

Figure 9: *Backpropagation. The pressure at P is to be expressed in terms of the pressures over the plane S' at later times.*

Suppose now that we have a general pressure field (i.e. not necessarily monofrequency)

$$p(\mathbf{r},t)=\int p_f(\mathbf{r})e^{j2\pi ft}df$$

By forming the Fourier frequency integral of (G.1), we see that the result for $p(\mathbf{r},t)$ is equal to a superposition of waves, $R^{-1}\exp j2\pi(\kappa R+ft)$ (see integrand of Eqn G.1), each modulated by the slowly-varying cosine function of position. The signs preceding κR and ft tell us that the wave is a collapsing one and so the waves propagate backwards in time. The resulting formula for $p(\mathbf{r},t)$ can be manipulated to yield the following more simple form

$$p(\mathbf{r},t)=\frac{1}{2\pi c}\int\cos(\hat{n},\mathbf{r}-\mathbf{r}')\frac{1}{R}\left[\frac{\partial p}{\partial t}\right]_{\mathbf{r}',t+R/c}dS' \qquad \text{(G.2)}$$

The evaluation at the advanced time $t+R/c$ reflects the backward nature of the propagation. Equation (G.2) is the generalisation of (G.1) to the general or non-monofrequency case.

Equation (G.2) bears a striking resemblance to the image-forming equation (2.7), despite the superficial differences. The resemblance is significant because, in (G.2), the backpropagated wave must obey true energy conservation. Let us see what differences, if any, between the two equations are truly 'essential.'

The differences can be classified as follows. The first group of differences are somewhat trivial: the cosine factor, the $1/R$ factor and the use of the time derivative. All these features in (G.2) can be matched by making the corresponding changes in the formula (2.7); and the images produced would be changed in only minor ways. Second, there are differences between, in (2.7), summing or integrating over an *array* (bounded in space, discrete elements) and, in (G.2), integrating over an effectively infinite, and continuous, surface. But an array has always been recognised as some kind of approximation to the full surface; the effects of the approximation, such as the nonzero beamwidth, are well known. Furthermore if one were to backpropagate from an array according to (G.2) but with obvious modifications, while there would be some blurring, etc. of the field, energy conservation would still hold. Hence this second group of differences is also unimportant in a sense.

The third group consists of three differences: (i) backpropagation deals with a passive system, not a two-way system; (ii) the formula (G.2) gives a time-dependent quantity $p(\mathbf{r},t)$, in contrast with the time-independent image amplitude $A(\mathbf{r})$; and (iii) in (G.2) neither reflectors nor sources are assumed present.

It will be argued that (ii) and (iii) flow logically from (i), as follows. In the two-way case, for a given position $\mathbf{r}$, the time t_0 at which the pulse is transmitted leads to a definite time

$$t_0+|\mathbf{r}-\mathbf{r}_t|/c \qquad \text{(G.3)}$$

at which the reflected signal should be evaluated to obtain the image amplitude $A(\mathbf{r})$. Such a definite time is missing in the passive case, where the times of emission from sources are in general not known. Thus the difference (ii) is a logical consequence of the difference (i), not an independent difference. We turn to the difference (iii). Here the presence of sources cannot be readily incorporated in the one-way case, for the very reason that there is no way to associate the value of $\mathbf{r}$ with a particular value of t. Again (iii) flows from (i).

Thus, among all the three groups of differences, *the only essential difference is between a two-way and a one-way system.* Then (Section 8.3) it is required to show that, in the one-way system, the image-forming procedure (2.7) is equivalent to physical backpropagation, as described by (G.2), apart from inessential differences. But this is what the discussion of differences has already shown.

Appendix H: Extension of Point-Target Proof to the Extended Model

As stated in Section 8.5, the proof will now be extended.

H.1. Transmitter Not in Array Plane

In Section 5.1 we considered the situation where the transmitter is displaced from the array plane. For convenience we took the state with the transmitter at the centre of the array as the basis for comparison; here we continue to do this. For a transmitter displaced from the centre, when (D.3) is substituted into the Equation (8.1) giving the array integral J_a, by translation of the variable of integration, it follows that J_a has the same value as for a non-displaced transmitter. Again, when (5.2) is substituted into (8.2) for the image integral J_i, it follows immediately that J_i is unchanged by the displacement of the transmitter. Hence the ratio J_i/J_a is unchanged. Hence the integral relationship (8.3) holds for the displaced transmitter as well as for the transmitter at the centre of the array—for a point target. This result is subject to the conditions given in Section 5.1.

H.2. Spherical Transmitter

On this occasion it is worth considering a general scene, since Equations (5.6) and (5.7) continue to hold for such a scene. In (8.1), it follows immediately from (5.6) that J_a for a spherical transmitter has the same value as for a point transmitter at the same point. Similarly in (8.2), from (5.7), J_i has the same value as for a point transmitter. Hence for a general scene we may say that the integral relationship (8.3) holds for a spherical transmitter *if* it holds for a point transmitter centred *at the same point*.

We now want to drop the qualifying 'if' clause. To this end, let us restrict attention to a point target. Subject to the conditions in Section 5.1, the integral relation does indeed hold for the point transmitter at the same point—which need not be in the array plane (as we saw in Section H.1). Hence the integral relationship (8.3) indeed holds for a spherical transmitter. This result is subject to the conditions of Section 5.1; the latter may be dropped if the transmitter is in the array plane.[44]

[44] At this stage we can also say, for a *collection* of point targets, that the integral relationship holds for a spherical transmitter *if* it holds for a point transmitter, provided both are located in the array plane.

H.3. Correlated Signal

Again we consider first a general scene. As discussed in Section 5.3, given the scene and the non-waveform parameters, both the $E_n(t)$ and $A(\mathbf{r})$ are determined by $\xi(t)$ in the uncorrelated case; in the correlated case they are determined via the *same* functional relationship but with $Y(t)$ replacing $\xi(t)$. This is true, not only of $E_n(t)$ and $A(\mathbf{r})$, but also of J_a and J_i in Equations (8.1) and (8.2). Furthermore we have imposed the *same* condition (5.13) on $Y(t)$ as on $\xi(t)$ (Eqn 4.4). Hence, *if* the integral relationship holds for an uncorrelated pulse, it also holds for a correlated one—this is for a general scene.

For a point scatterer therefore, the integral relation does hold for a correlated pulse. When the extensions in Sections H.1 and H.2 are also made, the conclusions given in those sections hold for correlated as well as uncorrelated signals.

Appendix I: Calculation of J_a for a Rough Surface

For a surface described by a reflection coefficient, it was shown in Section 7.2 that the squared modulus of the voltage stream is given by (7.15). Towards obtaining J_a (8.1), we note from (7.15) and (4.3) that

$$\int \left|E_n(t)\right|^2 dt = (D_r \sigma_n H)^2 T_e \pi^{-1} \int \rho \cos i \cos R \, dS \tag{I.1}$$

Note that the complications involving time delays drop out. We now assume that i, R and g in $\rho(i, R, g)$ may be evaluated at the centre of S (for the given n); and we proceed similarly for the factors $\cos i$ and $\cos R$. In other words, ρ, $\cos i$ and $\cos R$ are assumed to be constant over the surface S. The conditions for this assumption have already been imposed[45] at Equation (7.10). Consequently (I.1) becomes

$$\int \left|E_n(t)\right|^2 dt = (D_r \sigma_n H)^2 T_e \pi^{-1} S \rho_n \cos i \cos R_n \tag{I.2}$$

where the dependence of ρ and R on n has been retained and has been shown by means of subscripts.

We now sum to obtain J_a (8.1). Since the array is small compared to the range, the *relative* variation in $\cos R_n$ across the array is small, except when R_n is near 90°. We therefore put $R_n = R$, independent of n. Thus

$$J_a = \sum_n w_n^2 \int \left|E_n(t)\right|^2 dt = (D_r \sigma_{\text{rms}} H)^2 T_e \pi^{-1} S (\cos i \cos R) \sum_n w_n^2 \rho_n \tag{I.3}$$

In the experiment, the data from one geometrical arrangement are normally used to estimate a *single* value of ρ; it is assumed that all the ρ_n are equal. Thus finally, J_a is given by Equation (8.5).

The condition required for that last approximation (all ρ_n are equal) is essentially as follows. Let w be the 'width' of the curve of ρ versus R, i.e. the change ΔR that causes ρ to change appreciably. The condition is

$$w r_0 >> L \tag{I.4}$$

where r_0 is the range of the reflector. This condition is expected to hold except for near-specular reflectors; thus the approximation should generally be good. It is most likely to fail

[45] That set of conditions needs to be strengthened if w, defined below as the 'width' of the curve of ρ versus R, is small compared to $\pi/2$. The strengthening is done by imposing conditions of the same form as (I.4).

when the surface approximates a specular reflector and when furthermore the alignments are such that the 'specularly reflected' beam meets the array. This second requirement means[46] $R \approx i$, $g \approx 0$. Then a part of the array may receive the 'specular reflection' while the rest of the array receives a much lower intensity.

Under the latter circumstances, a comparison of (I.3) with (8.5) shows that the experiment will yield as the measured ρ the average reflection coefficient given by $\rho_{av} = \sum_n w_n^2 \rho_n / \sum_n w_n^2$. Note that in reaching this conclusion, two key assumptions have been made: (i) that the integral relation used in the experimental analysis holds, and (ii) that coherence (Section 7.1) does not cause a departure from the theory.

[46] The experiment is set up so that $R \approx -i$, $g \approx 0$; so that the second requirement reduces to $i \approx 0$.

DISTRIBUTION LIST

Theory Pertaining to Comparison and Calibration in an Experiment to Measure Acoustic Reflection Coefficients

David G. Blair

AUSTRALIA

DEFENCE ORGANISATION

Task Sponsor
DGMD

S&T Program
Chief Defence Scientist
FAS Science Policy
AS Science Corporate Management
Director General Science Policy Development
} shared copy
Counsellor Defence Science, London (Doc Data Sheet)
Counsellor Defence Science, Washington (Doc Data Sheet)
Scientific Adviser to MRDC Thailand (Doc Data Sheet)
Scientific Adviser Joint
Navy Scientific Adviser
Scientific Adviser - Army (Doc Data Sheet and distribution list only)
Air Force Scientific Adviser
Director Trials

Aeronautical and Maritime Research Laboratory
Director

Chief of Maritime Operations Division
Research Leader Mine Warfare
Dr B Ferguson, MOD Sydney
Dr Kam Lo, MOD Sydney
Stuart Anstee, MOD Sydney
Roger Neill, MPD Melbourne
Ross Barrett, MOD Salisbury
David Kershaw, MOD Salisbury
Darryl McMahon, MOD Stirling
David Blair (Author): 12 copies

ESRL
Alan Burgess, LOD Edinburgh
Garry Newsam, SSD Edinburgh

DSTO Library and Archives
Library Edinburgh 1 copy
Australian Archives
Library, MOD, Pyrmont
US Defense Technical Information Center, 2 copies

UK Defence Research Information Centre, 2 copies
Canada Defence Scientific Information Service, 1 copy
NZ Defence Information Centre, 1 copy

Capability Systems Staff
Director General Maritime Development
Director General Aerospace Development (Doc Data Sheet only)

Knowledge Staff
Director General Command, Control, Communications and Computers (DGC4) (Doc Data Sheet only)

Navy
SO (SCIENCE), COMAUSNAVSURFGRP, NSW (Doc Data Sheet and distribution list only)

Army
ABCA National Standardisation Officer, Puckapunyal (4 copies)
SO (Science), Deployable Joint Force Headquarters (DJFHQ) (L), Enoggera QLD (Doc Data Sheet only)
NPOC QWG Engineer NBCD Combat Development Wing, Puckapunyal, VIC (Doc Data Sheet relating to NBCD matters only)

Intelligence Program
DGSTA Defence Intelligence Organisation
Manager, Information Centre, Defence Intelligence Organisation

Corporate Support Program
Library Manager, DLS-Canberra
MS Sam Doran, Defence Library Service - Sydney West

Acquisitions Program
Acoustic Mine Imaging Project Manager, Dept of Defence, Russell Offices, R2-3-C059, Canberra

UNIVERSITIES AND COLLEGES
Australian Defence Force Academy
Library
Head of Aerospace and Mechanical Engineering
Hargrave Library, Monash University (Doc Data Sheet only)
Librarian, Flinders University

OTHER ORGANISATIONS
NASA (Canberra)
AusInfo
Mr Neil Hodges, AMI Manager, Thales Underwater Systems, 274 Victoria Rd, Rydalmere, NSW 2116 (4 copies)
Dr Mark Hedley, AMI Manager, TIP Division, CSIRO, PO Box 76, Epping, NSW 1710 (3 copies)
Dr Bob Harrison, Manager NDE, ANSTO, New Illawarra Rd, Lucas Heights, NSW 2234 (2 copies)

Dr ISF Jones, Ocean Technology Group, J05, University of Sydney, NSW 2006
Dr Andrew Madry, Madry Technologies, PO Box 1269, Castle Hill, NSW 1765
Dr David Robinson, Pen-Y-Sarn, 383 Burraneer Rd, Coomba Park, NSW 2428
Dr EO Belcher, Applied Physics Laboratory, University of Washington, Seattle, WA, U.S.A.
Dr RK Hansen, Omnitech as, Nedre Astveit 12, N-5083 Ovre Ervik, Bergen, Norway
Dr J Impagliazzo, Naval Undersea Warfare Center, Newport, Rhode Island, U.S.A.
Dr PT Gough, Dept. of Electrical and Electronic Engineering, University of Canterbury, Private Bag 4800, Christchurch, N.Z.
Dr Leslie Kay (New Zealand), C/- Dr J Sendt, Thales Underwater Systems, 274 Victoria Rd, Rydalmere, NSW 2116

OUTSIDE AUSTRALIA

ABSTRACTING AND INFORMATION ORGANISATIONS

Library, Chemical Abstracts Reference Service
Engineering Societies Library, US
Materials Information, Cambridge Scientific Abstracts, US
Documents Librarian, The Center for Research Libraries, US

INFORMATION EXCHANGE AGREEMENT PARTNERS

Acquisitions Unit, Science Reference and Information Service, UK
Library - Exchange Desk, National Institute of Standards and Technology, US

SPARES (5 copies)

Total number of copies: 79

DEFENCE SCIENCE AND TECHNOLOGY ORGANISATION
DOCUMENT CONTROL DATA

1. PRIVACY MARKING/CAVEAT (OF DOCUMENT)

2. TITLE

Theory Pertaining to Comparison and Calibration in an Experiment to Measure Acoustic Reflection Coefficients

3. SECURITY CLASSIFICATION (FOR UNCLASSIFIED REPORTS THAT ARE LIMITED RELEASE USE (L) NEXT TO DOCUMENT CLASSIFICATION)

Document	(U)
Title	(U)
Abstract	(U)

4. AUTHOR(S)

David G. Blair

5. CORPORATE AUTHOR

Aeronautical and Maritime Research Laboratory
506 Lorimer St
Fishermans Bend Vic 3207 Australia

6a. DSTO NUMBER	6b. AR NUMBER	6c. TYPE OF REPORT	7. DOCUMENT DATE
DSTO-TN-0417	AR-012-280	Technical Note	March 2002

8. FILE NUMBER	9. TASK NUMBER	10. TASK SPONSOR	11. NO. OF PAGES	12. NO. OF REFERENCES
490-6-97	NAV 01/041	DGMD	84	26

13. URL on the World Wide Web

http://www.dsto.defence.gov.au/corporate/reports/ DSTO-TN-0417.pdf

14. RELEASE AUTHORITY

Chief, Maritime Operations Division

15. SECONDARY RELEASE STATEMENT OF THIS DOCUMENT

Approved for public release

OVERSEAS ENQUIRIES OUTSIDE STATED LIMITATIONS SHOULD BE REFERRED THROUGH DOCUMENT EXCHANGE, PO BOX 1500, SALISBURY, SA 5108

16. DELIBERATE ANNOUNCEMENT

No Limitations

17. CASUAL ANNOUNCEMENT Yes

18. DEFTEST DESCRIPTORS

Beam forming, Acoustic reflection, Acoustic imaging, Sonar arrays

19. ABSTRACT

For the purpose of analysing data to determine underwater acoustic reflection coefficients at low megahertz frequencies, relevant theory is developed. For a target that may be in the near field, the three-dimensional point spread function for image points close to the target, is derived for rather general arrays and waveforms. The model of the active system is extended to allow a coded signal, a spherical transmitter, and a transmitter not in the receiver array plane. Here and elsewhere, conditions of validity are carefully obtained. Conditions are derived under which a ball target (used for calibration in the experiment) behaves as a point reflector. The image of a rectangular target, described by an angle-dependent reflection coefficient, is obtained. The preceding results lead to an 'integral relationship,' or 'energy conservation' relationship, proved for a point target and conjectured to hold generally. It is shown how this result would enable one to analyse the experiment to determine absolute reflection coefficients.